OEA | Opto-Electronic Advances

Review

2026, Vol. , No.

Open Access

AI-assisted metaphotonics

Minsung Kang[1†], Seokju Choi[2†], Kaixi Fu[1], Xiaoyuan Liu[3], Zhun Wei[4], Lei Jin[5], Hao Wang[6,7], Olivier J. F. Martin[3], Joel K. W. Yang[8], Sunae So[2]* and Trevon Badloe[1,9,10]*

Abstract: The convergence of artificial intelligence (AI) and metaphotonics is creating a new paradigm for controlling light-matter interactions. The synergy of AI's ability to learn complex relationships in multidimensional data and provide ultra-fast inference with the capacity of metaphotonics to engineer optical properties not found in nature is unlocking a new era in computational design, real-time control, and fully automated optical systems. This review provides a comprehensive overview of state-of-the-art AI-driven approaches for metaphotonic systems. We focus on the solutions to real-world problems in accelerating metaphotonic simulations and inverse design, optical data characterization, and the development of fully integrated end-to-end AI-assisted metaphotonic systems. Finally, we provide our perspectives on the future research directions and emerging opportunities at the rapidly evolving intersection of metaphotonics and AI.

Keywords: metaphotonics; metasurfaces; metamaterials; artificial intelligence; machine learning

DOI: 10.29026/oea.2026.250263 | CSTR: 32247.14.oea.2026.250263

Citation: Kang M, Choi S, Fu K et al. AI-assisted metaphotonics. *Opto-Electron Adv*, 250263 (2026).

1 Introduction

Conventional bulk optical components, such as lenses and prisms, possess thicknesses and volumes far larger than the wavelength of light, thus creating physical constraints that increase the overall size and weight of optical systems. This inherently limits miniaturization and weight reduction for compact and portable optical solutions. Metasurfaces, composed of 2D planar arrays of subwavelength-scale meta-atoms, offer a promising approach for lightweight, multi-functional optical devices[1,2]. Governed by the generalized Snell's law, metasurfaces enable anomalous reflection or refraction, a feat that cannot be achieved by conventional refractive optics with introducing a phase gradient at the interface between two media[3]. This feature makes it possible to tailor the properties of light, such as phase, amplitude, and polarization, allowing the direct synthesis of arbitrary wavefronts.

With this high degree of freedom, metasurfaces have been investigated for a wide range of applications including flat lenses known as metalenses[4–9], holography[10–12], and structural color printing for high-resolution pigment-free coloration[13–17]. Despite these advantages, the design and optimization of metasurfaces still face inherent challenges. The optical properties of a metasurface are determined by numerous design parameters, including the geometry, size, material, and arrangement of the constituent meta-atoms. This makes it unreasonable to rely solely on traditional trial-and-error methods or intuitive physical insights for their design. Additional challenges including achieving

Received: 26 September 2025

Accepted: 9 January 2026

Published online: 4 March 2026

[1]Department of Electronics and Information Engineering, Korea University, Sejong 30019, Republic of Korea; [2]Department of Control and Instrumentation Engineering, Korea University, Sejong 30019, Republic of Korea; [3]Nanophotonics and Metrology Laboratory (NAM), Swiss Federal Institute of Technology Lausanne (EPFL), Lausanne 1015, Switzerland; [4]Innovation Institute of Electromagnetic Information and Electronics Integration, Zhejiang Key Laboratory of Intelligent – Electromagnetic Control and Advanced Electronic Integration, College of Information Science & Electronic Engineering, Zhejiang University, Hangzhou 310017, China; [5]Key Laboratory of RF Circuits & System of Ministry of Education, School of Electronics and Information, Hangzhou Dianzi University, Xiasha High Education Park, Hangzhou 310018, China; [6]School of Instrumentation and Optoelectronic Engineering, Beihang University, Beijing 100191, China; [7]Hangzhou International Innovation Institute, Beihang University, Hangzhou 311115, China; [8]Engineering Product Development, Singapore University of Technology and Design, Singapore 487372, Singapore; [9]Division of Smart Energy Convergence Engineering, Korea University, Sejong 30019, Republic of Korea; [10]Digital Healthcare Center, Sejong Institute for Business and Technology, Korea University, Sejong 30019, Republic of Korea.

†These authors contributed equally to this work.

*Correspondence: S So, E-mail: sunaeso@korea.ac.kr; T Badloe, E-mail: trevon@korea.ac.kr

uniformity and cost-effectiveness in large-area fabrication, as well as addressing non-intuitive design complexities, remain open as problems that are yet to be completely solved. These limitations have motivated growing interest in alternative methodologies that can efficiently explore large design spaces, capture complex structure–response relationships, and include physics-driven designs that consider real fabrication errors. Artificial intelligence (AI) stands out among the potential solutions.

Driven primarily by advances in deep learning, AI has emerged as a powerful tool that has achieved human-level, and in some cases superior, performance across diverse fields including computer vision, natural language processing, and drug discovery, leading to a fundamental paradigm shift in scientific problem-solving[18–20]. The value of AI has been recognized by nations worldwide and has been reflected by the formulation of national-level strategies and policies, reflecting the expansion of global AI competition beyond technological development into policy, education, and industry[21]. Considering the complexity of metasurface design and the analytical and optimization capabilities of AI, the integration of these two fields offers obvious complementary advantages.

As the research in metamaterials and metasurfaces has developed from fundamental science towards next generation technology[22], the field of 'metaphotonics' has emerged as a distinct discipline. While nanophotonics broadly describes light-matter interactions at the nanoscale, and metamaterials and metasurfaces refer to the 3D bulk and 2D planar architectures designed to exhibit artificial optical properties, metaphotonics encompasses the overarching field of applying these exotic subwavelength structures to manipulate light for advanced photonic systems. In this context, AI has rapidly emerged as a valuable tool for effectively addressing the wide range of inherent challenges in the field, from the design of meta-atoms and metasurfaces to optical output analysis (Fig. 1). In this review, we discuss how AI has been implemented in metasurface computational design and optimization, and highlight the current challenges faced by integrating AI into inverse design for real-world applications. We then move onto the use of AI for the characterization, analysis, and interpretation of optical information obtained from metasurfaces, where the power of AI is used to understand multidimensional spectral or image data. We introduce the latest advancements in end-to-end and AI-integrated metaphotonic systems that consider the entire design and data acquisition processes in a fully differentiable pipeline, as well as sense, react, and respond to external stimuli and modulate their optical output in real time. We conclude the review with a perspective on the future potential research directions in the fields of AI-assisted metaphotonic systems and provide a brief overview of the potential of metaphotonics hardware for AI applications.

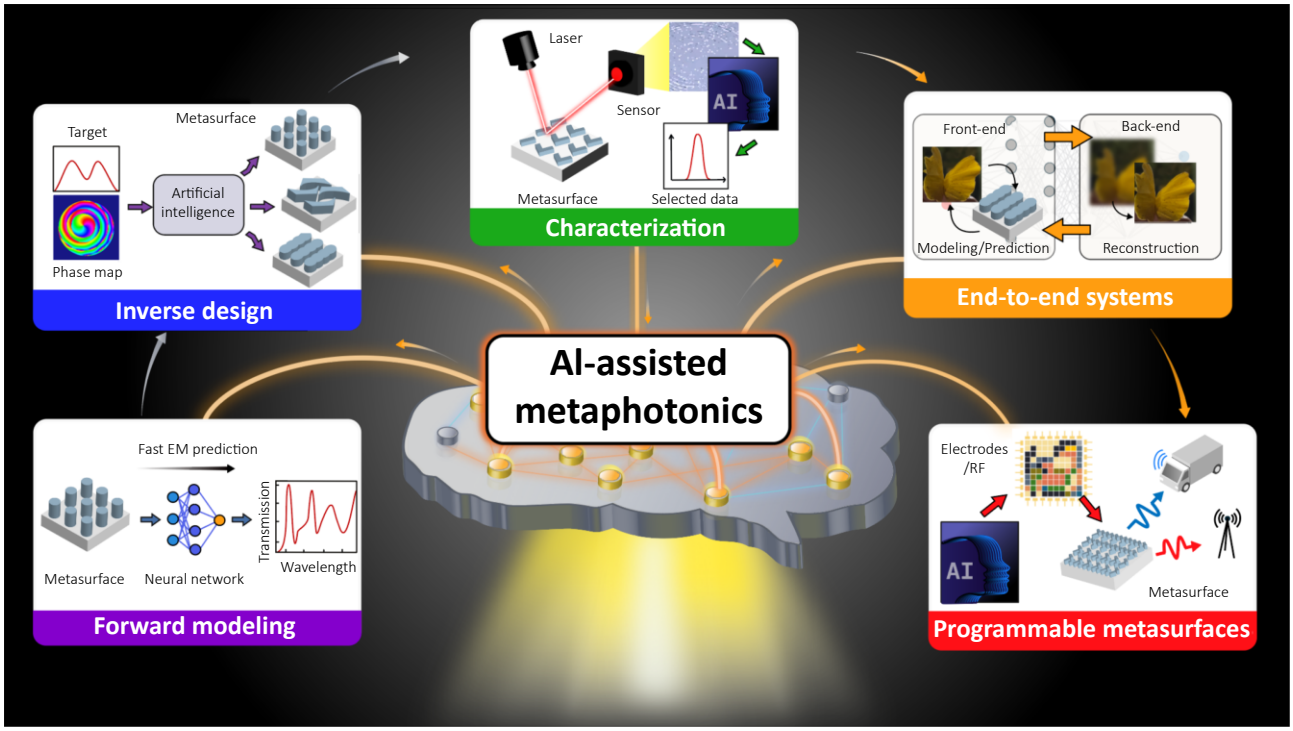

Fig. 1 | Schematic illustration of AI-assisted metaphotonic systems. AI serves as a valuable tool for metaphotonic systems, enabling the optimization and design of metasurfaces, the characterization and interpretation of multidimensional optical data, as well as end-to-end design, analysis, and the powering of fully autonomous optical systems.

2 AI for metasurface design and optimization

2.1 AI-powered surrogate models

Metasurface design relies on the calculation of electromagnetic responses to precisely control the optical properties of light at will. Conventional techniques, including the finite-difference time-domain (FDTD) method, finite element method (FEM), and rigorous coupled-wave analysis (RCWA), numerically or semi-analytically solve Maxwell's equations to yield high-accuracy results. While such simulations are computationally feasible for meta-atoms made up of simple cross-sections, they become time-consuming as the meta-atom complexity increases. Resolving fine structural features necessitates an increasingly fine spatial and temporal discretization, leading to substantial computational costs and limiting the feasibility of large-scale simulations.

To address these limitations, AI-driven surrogate models have emerged as powerful tools to map metasurface geometries directly to electromagnetic responses (Fig. 2(a)), achieving predictions that are several orders of magnitude faster than conventional full-field methods while maintaining comparable accuracy[23]. Surrogate models are trained on a limited set of high-fidelity simulations, which allows them to rapidly infer the electromagnetic behavior of new structures within the training domain without the need for costly full-wave simulations. These surrogate models can then be implemented directly into optimization algorithms for extremely fast simulation results. Such models are particularly effective when the metasurface geometry is represented as a spatially structured input, preserving both local and global geometric context and enabling the model to capture complex interactions across multilayer or even freeform layouts[24,25]. A common implementation employs a three-dimensional voxel grid, in which each voxel encodes the local material properties. In such cases, convolutional neural networks (CNNs) are frequently employed[26–28]. For instance, Wiecha et al.[29] reported a CNN that extracts features at multiple levels: early layers capture interfaces and layer boundaries, while deeper layers learn resonant patterns and longer-range field correlations. By leveraging localized receptive fields and weight sharing, their CNN-based surrogate models delivered near-instantaneous predictions once trained, achieving a 3 to 5 order-of-magnitude speed-up in predicting the electric field. While surrogate models generalize effectively to structures within the training distribution, their predictive accuracy deteriorates sharply when confronted with inputs outside this domain, reflecting their reliance on data-driven statistical correlations rather than explicit physical laws.

Neural-operator-based models[30,31] offer a complementary paradigm by learning continuous mappings between infinite-dimensional function spaces rather than between fixed-size vectors. In this framework, an operator $\mathcal{G}$ transforms an

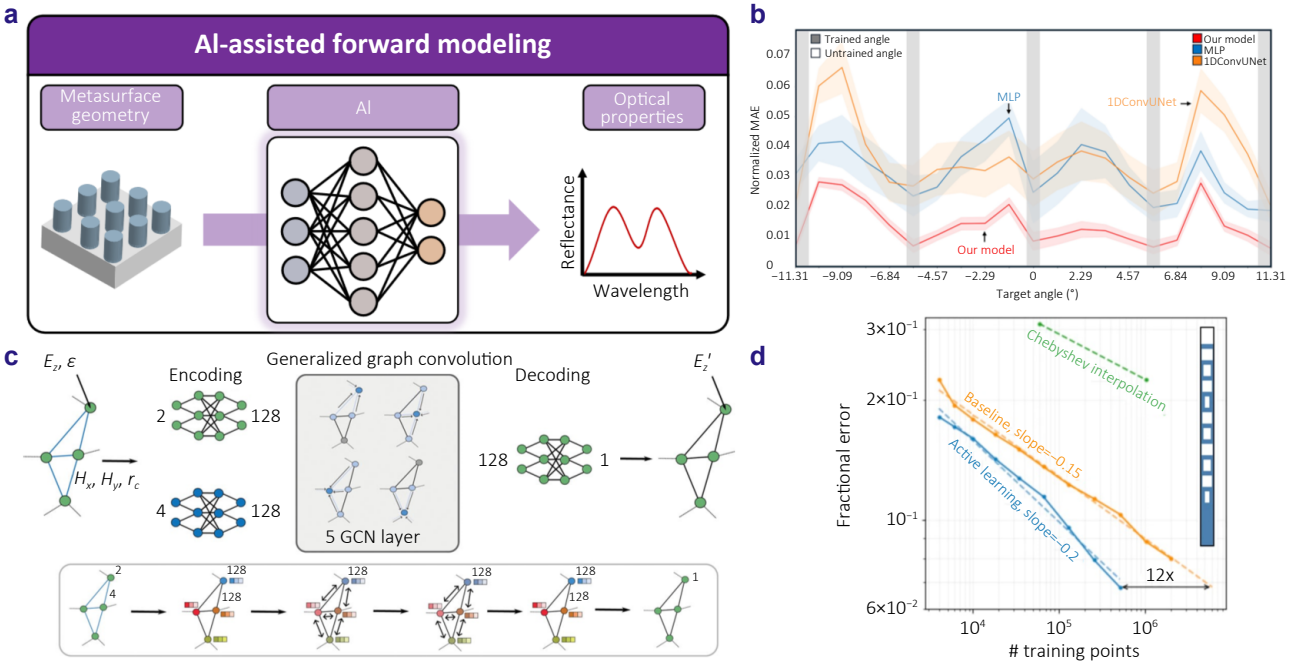

Fig. 2 | Surrogate AI-models for nanophotonic simulations. (a) Schematic illustration of AI-powered forward simulation of the optical properties of metasurfaces. (b) Accurate prediction of adjoint gradients for untrained angles by the Fourier neural operator (FNO), outperforming a multilayer perceptron (MLP) and a conventional convolutional neural network (U-Net) through continuous function. (c) The overall architecture and message passing mechanism of a GNN. (d) A comparison of test error between an actively learned surrogate model and a baseline model using random sampling. Figure reproduced with permission from: (b) ref. [31], (c) ref. [34], (d) ref. [35], under a Creative Commons Attribution License.

input function $f(x)$, such as a spatial permittivity distribution, into an output function $u(x) = \mathcal{G}(f(x))$, e.g., the resulting electromagnetic field. By approximating $\mathcal{G}$ directly, these models can accept arbitrary samplings of $f(x)$ on two- or three-dimensional grids and produce $u(x)$ on the same or different grids without retraining. This functional representation encodes physical relationships more naturally and enables generalization across varying material properties and domain sizes as the model learns a mapping from a spatial distribution of physical parameters such as permittivity to the electromagnetic response. Consequently, different materials can be readily evaluated by specifying their permittivity values in the input function, bypassing the need for retraining (Fig. 2(b)). For instance, Augenstein et al.[30] demonstrated that the Fourier neural operator maintains stable accuracy and tightly clustered prediction errors even under out-of-distribution conditions, highlighting its robust generalization capabilities. Nevertheless, since both the inputs and outputs remain discretized on fixed grids, curved or irregular boundaries are inevitably represented as a series of stepwise approximations. This staircasing effect can introduce local geometric inaccuracies, which in turn may distort electromagnetic interactions and compromise the fidelity of the simulation in regions with fine structural details.

To overcome such limitations, graph neural networks (GNNs)[32] have been introduced to accurately capture curved or irregular boundaries. In this framework, a photonic structure is represented as a graph, where nodes correspond to individual meta-atoms[33] or discrete spatial points[34], each storing information such as local field values, permittivity, and geometric parameters. Edges connect neighboring nodes based on physical proximity, encoding coupling strength, distances, and boundary conditions. Through iterative message passing, nodes exchange information with their neighbors, progressively capturing both local and long-range electromagnetic interactions across the structure (Fig. 2(c)). This graph-based representation enables GNNs to naturally handle curved boundaries, irregular geometries, and complex meshes without the limitations inherent in grid-based models. Khoram et al.[33] demonstrated that a GNN could accurately predict near-field distributions for a large elliptical metasurface with void regions with less than 5% error compared to FDTD, while reproducing far-field holograms with over 98% fidelity at a distance of 30 λ. These predictions required only seconds of computation, in contrast to the minutes needed for conventional solvers. Such results highlight the ability of GNNs to respect fundamental physical laws while providing fast, high-fidelity generalization across metasurfaces of arbitrary scale and morphology. Nevertheless, despite their advantages in boundary representation, GNN-based surrogate models that compress metasurface geometries and field data into low-dimensional latent spaces demand large, high-quality datasets from extensive full-wave simulations or costly experiments to learn stable and generalizable representations. Consequently, data acquisition remains a critical bottleneck for scaling these methods to increasingly complex designs.

To mitigate training data limitation challenges, data-efficient learning strategies such as active learning[35] and transfer learning[36] have been employed. Active learning allows a model to proactively select the most informative samples, prioritizing regions of high predictive uncertainty or areas likely to yield maximal performance gains. These selected samples are then labeled via simulations or experiments and incorporated into training iteratively, ensuring the model focuses only on the most valuable data points while avoiding redundancy. This advantage has been demonstrated by Pestourie et al.[35], who achieved a fractional error of 0.07 while using twelve times fewer sample points than random selection, dramatically reducing data requirements (Fig. 2(d)). Complementing this, transfer learning[37] leverages prior knowledge from related tasks to accelerate and stabilize training when datasets are limited. Rather than initializing models from scratch, transfer learning adapts layers pretrained on a source domain to a target task, reducing training time and improving generalization. For example, in multilayer thin-film spectrum prediction, Qu et al.[37] demonstrated that reusing a small set of early layers and fine-tuning all weights reduced test errors by approximately 50% for eight-layer stacks and 25% for ten-layer stacks, highlighting the effectiveness of hierarchical feature reuse. Together, active learning and transfer learning form a synergistic framework, where active learning guides data acquisition, and transfer learning maximizes prior knowledge, enabling high-fidelity modeling under stringent data constraints.

Collectively, recent advancements address four central challenges in AI-driven surrogate models: 1) grid-based surrogates accelerate electromagnetic predictions; 2) neural operators maintain accuracy across varying grid resolutions without retraining; 3) graph-based models faithfully represent curved boundaries and complex geometries, and 4) data-efficient learning strategies reduce the demand for large training datasets. With these advancements, recent surrogate models provide a robust foundation for inverse design, facilitating the engineering of metasurfaces that meet precise performance specifications, which will be discussed in the following section. The key characteristics, suitable geometries, and limitations of these surrogate modeling strategies are summarized in Table 1.

2.2 Empowering inverse design

Inverse design leverages computational frameworks to identify structural parameters of meta-atoms or metasurfaces that achieve predefined optical targets. Early approaches implemented deep neural networks (DNNs) to directly map target optical responses, such as phase profiles[38], transmittance spectra[39], or far-field holograms[40], to design parameters

Table 1 | Comparison of AI-assisted forward modeling approaches for nanophotonic simulations.

Model	Speed	Data efficiency	Suitable geometry	Limitations
Conventional solvers (FDTD, FEM, RCWA)	High cost for finely meshed complex structures	No training data required	Structured grids (FDTD, Yee cell), unstructured meshes (FEM), and layered periodic structures (RCWA)	Poor scalability in memory and runtime for large domains
CNN-based[26–29]	Orders-of-magnitude faster than full-wave solvers (e.g., 3–5 orders[29])	Moderate	Voxelized, multilayer, freeform on grids	Poor out-of-distribution generalization
Neural operator[30,31]	Fast inference, resolution-independent	Moderate	Variable grids and materials	Staircasing at curved boundaries
GNN[32–34]	Significant acceleration (e.g., seconds instead of minutes for large metasurfaces[33])	Large dataset required	Curved, irregular geometries	Data-acquisition bottleneck
Active learning[35]	Reduces simulation overhead (e.g., 12× fewer samples[35])	High	Model-agnostic	Iterative workflow complexity
Transfer learning[36,37]	Accelerates training (e.g., ~50% error reduction[37])	High	Related source-target tasks	Requires related source domain

(Fig. 3(a)). However, the intrinsic one-to-many nature of such mappings often resulted in unstable or non-convergent training. To mitigate this issue, tandem architectures were introduced, in which an inverse network is coupled with a pretrained surrogate forward model[41–42]. By minimizing reconstruction error between predicted and target optical responses, this framework stabilizes learning and improves predictive fidelity within the training domain of the surrogate model. Complementing purely data-driven approaches, researchers have also integrated surrogate forward models with classical optimization algorithms to enable broader exploration of the design space beyond the constraints of pre-defined networks[43–46]. For instance, Hemayat et al.[47] employed a high-speed surrogate model within a particle swarm optimization framework, effectively replacing computationally expensive full-wave evaluations. This surrogate-in-the-loop optimization reduced per-design evaluation times from approximately 56 hours to 0.08 seconds, facilitating parallel exploration and rapid convergence. Similarly, Li et al.[48] combined a neural surrogate with a genetic algorithm, allowing the optimizer to query fast predictions instead of performing full-wave simulations, while maintaining amplitude and phase errors below 3%. Despite their remarkable acceleration of the inverse design process, these surrogate-driven optimization schemes remain inherently limited by the parameterization of the underlying structure libraries. As a result, they excel at efficiently navigating known design spaces but offer restricted capacity for discovering fundamentally novel metasurface geometries.

Probabilistic generative models have emerged as a powerful approach for exploring the multiplicity of valid solutions inherent to inverse metasurface design. Among these, generative adversarial networks (GANs) facilitate the generation of diverse candidate structures that all satisfy a given optical target, effectively providing a richer distribution of feasible designs. Unlike deterministic inverse mappings, which yield a single solution, GANs enable the exploration of the design space, thereby enhancing robustness and providing a broader set of options for selection[49,50]. For example, a GAN was demonstrated to inversely design free-form nanophotonic antennae from a desired reflection spectrum[24], successfully generating novel structures unconstrained by predefined shapes. Stanley et al.[51] employed a GAN framework that allows the generator to assign materials at each spatial location via a compact mathematical network, allowing complex patterns to emerge organically without ever simulating how regions grow or interact over time. Despite these advantages, GANs are susceptible to training instability, impeding convergence to a stable solution, and also prone to mode collapse, producing only a few highly similar designs rather than sampling the full distribution[52]. Both issues originate from the adversarial training process. Originally developed in machine learning for generative tasks, diffusion models have recently been introduced to mitigate the stability and diversity limitations inherent to GANs[53]. Compared to adversarial or autoencoder-based surrogates[54], this diffusion-based approach has been shown to achieve higher accuracy with minimal structural artifacts, demonstrating both robustness and fidelity in pattern generation (Fig. 3(b)). To bring together the stability of tandem networks, the diversity of GANs, and the accuracy of diffusion models, a hybrid approach has been proposed[55]. A coarse structure was first generated by a tandem network, followed by a greatly reduced number of diffusion steps to shape the overall geometry, and finally refined using a lightweight adversarial discriminator to enhance high-frequency details. This hybrid strategy accelerates design generation more than tenfold compared to pure diffusion models, while maintaining low reconstruction error and stable convergence.

Accurate and reliable predictions are crucial in metasurface inverse design, as even small modeling errors can lead to significant performance degradation or fabrication failures in practical devices. One effective strategy to achieve

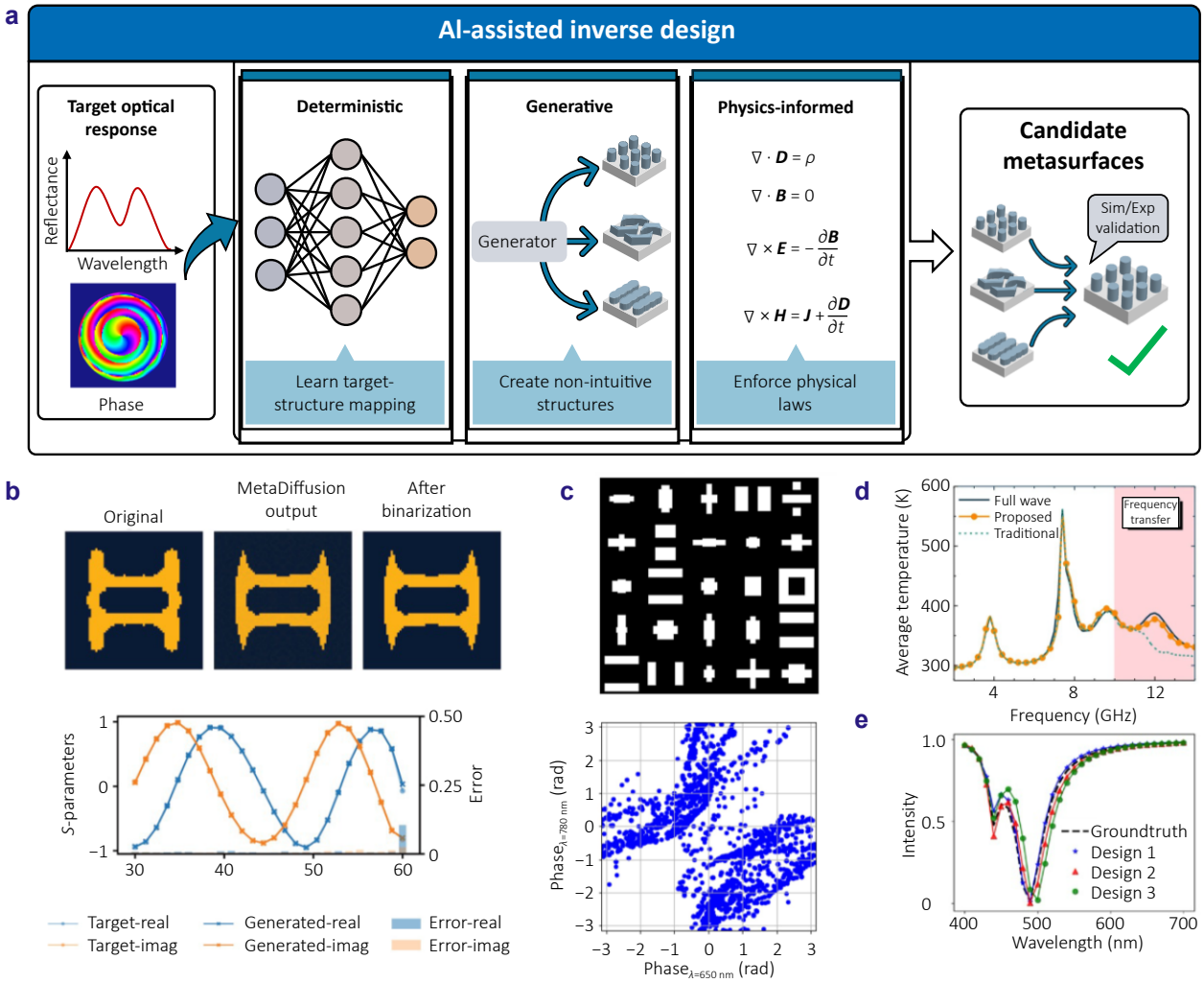

Fig. 3 | Metaphotonic inverse design powered by AI. (a) Schematic illustration of AI-driven inverse design for metasurfaces. (b) The mean absolute error on the entire test set of inverse designed metasurfaces using diffusion models. (c) Phase coverage of meta-atoms selected considering fabrication tolerances. (d) Performance evaluation of AI-models capable of frequency transfer outside of the training data region. (e) The transmission spectra of three different metasurface structures generated by a fine-tuned LLM via inverse design. Figure reproduced with permission from: (b) ref.[53], (c) ref.[77], (d) ref.[82], (e) ref.[88], under a Creative Commons Attribution License.

this reliability is to embed physical laws directly into the model, constraining the solution space to physically admissible outcomes. This approach improves data efficiency, generalization, and interpretability[56–58]. For example, adjoint-based shape and topology optimization frameworks have been used to select metasurface geometries consistent with Maxwell's equations and material anisotropy, enforcing ideal phase targets while prioritizing dominant local coupling[59,60]. This physics-informed pruning effectively reduced the number of required labels by approximately two- to tenfold compared with purely data-driven methods, while maintaining fabrication tolerances.

Physics -informed neural networks (PINNs) extend this idea by incorporating the governing physics directly into the training process. By adding a term for the partial-differential-equation residual, such as the Maxwell equations or the Helmholtz equation, to the loss function[61], PINNs guide the model toward solutions that inherently satisfy the physical laws. For instance, Medvedev et al.[62] developed a PINN that requires no labeled simulation pairs. The loss includes the residual of the three-dimensional vector Maxwell equations, together with Floquet–Bloch boundary conditions and perfectly matched layers. Evaluated at collocation points defined by coordinates, material parameters, and boundary conditions, the network is penalized whenever the physics are violated. This physics-driven supervision reduces dependence on labeled data while producing millisecond-scale scattering predictions that generalize well to unseen geometries and illumination conditions. While PINNs provide additional constraints that ensure that the models adhere to physical laws, a limitation exists whereby too much physics would cause an AI model to simply become an expensive to

train physical approximation of laws that we already know.

Beyond ensuring physical consistency and data efficiency, embedding physical laws into the model also enhances interpretability, addressing the limitations of black-box models that obscure the causal relationships between designs and performance[63]. For example, Shao et al.[64] incorporated the electromagnetic principles of wave propagation, local modulation, and the Huygens-Fresnel superposition directly into the network design. Propagation was modeled as a complex-valued linear operation based on Maxwell's equation analysis, preserving phase accumulation, while local modulation was represented as a real-valued nonlinear transformation to capture amplitude and phase alterations induced by material and geometry. The superposition principle was explicitly applied to reconstruct the overall wave field from individual segments responses. By embedding these physical laws, each output can be traced to its underlying mechanism, enabling both interpretability and physically consistent predictions. This approach complements the data efficiency and physical interpretability, thereby enhancing the reliability of designs that can be translated into the practical fabrication of complex optical structures.

In summary, the evolution of inverse design methods has progressed from deterministic deep network mappings to surrogate-driven optimization, GAN-based generation, diffusion-model refinement, hybrid frameworks, and PINNs that integrate stability, diversity, and speed. Future directions include the integration of active learning to continuously improve surrogate model accuracy, and the adaptation of advanced generative models[65] for even more flexible and high-fidelity exploration of the one-to-many design landscape. It is important to highlight here that such AI-based optimization is still a data-driven approach, so it cannot be guaranteed that the result is the global maximum or minimum. However, after showing great promise in theory, real-world challenges pose stronger limitations on the realization of the designed devices. A side-by-side comparison of the speed, design diversity, physics embedding, and limitations of these representative inverse-design methods is provided in Table 2.

2.3 Addressing real-world design challenges

Despite the rapid advances in computational inverse design, deploying AI-driven metasurfaces in practice presents several critical challenges. A primary concern is the ability of a model to generalize from training data that is often limited, biased, or computationally expensive to generate using full-wave simulations. Furthermore, designs are fundamentally constrained by the realities of physical fabrication, such as minimum feature sizes, alignment tolerances, and material imperfections. Scaling these designs to larger areas introduces additional computational and memory demands. Beyond physical constraints, the utility of the models themselves presents hurdles. The "black-box" nature of many AI models hinders interpretability, while their transferability to new wavelengths, materials, or geometries is often limited without extensive retraining. Finally, the entire process demands substantial expertise in both physics and computational programming, creating a high barrier to entry for non-specialists. In the following subsection, we explore strategies to mitigate these challenges, from data-efficient modeling to physics-informed constraints, facilitating the translation of inverse-designed metasurfaces to real-world applications.

2.3.1 Data and fabrication constraints

Deep-learning models for metasurface design must learn highly complex, nonlinear mappings between structural geometries and electromagnetic responses. In practice, however, obtaining sufficient high-quality training data is challenging. Limited datasets often lead to overfitting, causing models to generalize poorly to unseen structures and omitting essential physical modes in the design predictions[66,67]. While typical datasets contain tens of thousands of samples, a small 30 × 30-pixel freeform pattern metasurface exceeds 10^{270} possible configurations. Given this, evaluation via full-wave simulations is infeasible, highlighting the need

Table 2 | Comparison of inverse design methods for metasurfaces.

Method	Speed	Design diversity	Physics embedding	Limitations
Direct DNN[38–40]	Fast inference	Single solution	None	Unstable training (one-to-many)
Tandem network[41,42]	Fast inference with stable training	Single solution	Implicit (surrogate)	Limited to surrogate domain
Surrogate-driven optimization [43–45,47,48]	Significant acceleration (e.g., 56 h → 0.08 s[47])	Multiple candidates	Implicit (surrogate)	Predefined parameterization only
GAN[24,49–52]	Fast sampling	High (freeform)	None	Mode collapse; training instability
Diffusion model[53,54]	Slow sampling	High	None	Computationally expensive
Hybrid inverse design (Tandem + diffusion + adversarial refinement)[55]	Faster than pure diffusion (e.g., >10× [55])	High	Implicit	Architectural complexity
Physics-informed[56–59,61–64]	Moderate to fast (e.g., ms-scale[62])	Physically constrained	Explicit (PDE, adjoint)	Behaves close to a traditional physics solver

for strategies that enhance data efficiency and enable robust learning under sparse-data conditions.

To address the challenges posed by limited data, researchers have developed strategies to augment and expand available datasets while preserving key physical characteristics[68,69]. For instance, Zhang et al.[26], generated a design pool of 51,000 free-form chiral metasurface samples through full-wave electromagnetic simulations. During the iterative process of creating these samples, they augmented selected subsets of high-performing data using geometric transformations, such as rotation and reflection, to effectively train the generative model. These transformations preserved the fundamental chiroptical properties while varying orientations and arrangements, enabling neural networks to learn richer and more robust features at minimal computational cost. Nonetheless, such straightforward augmentations cannot fully capture the intricate, irregular boundary features that critically influence device performance, highlighting the need for more advanced data-efficient strategies.

Generative approaches, such as attention-guided diffusion models, have emerged as a powerful solution for extrapolating beyond limited training data[70]. By conditioning the generation on target performance and incorporating attention mechanisms, subtle electromagnetic response patterns can be captured to enrich the design space with high-performance candidates. First, multi-objective optimization methods were used to select top-performing candidate geometries, then attention-guided diffusion models were used to generate entirely new structures that surpass the performance of the initial dataset. While these strategies significantly improve design fidelity under limited-data conditions, models trained solely on ideal simulations may still face challenges when applied to experimental scenarios, motivating the integration of realistic noise and measurement-informed data to bridge the simulation-to-real gap.

Experimental imperfections, including fabrication variability, noise, and optical blur, can significantly degrade design fidelity. Ding et al.[71] addressed this by enriching simulated metasurface responses with experimentally measured sensor noise and calibrated optical blur, ensuring that the augmented simulations reflected the point-spread function of the system across wavelengths. Training on these noise-enhanced simulations mitigated overfitting to ideal data and enabled robust spectral reconstructions under realistic laboratory conditions. Complementing augmentation strategies, high-throughput fabrication and measurement pipelines have been employed to systematically generate extensive experimental datasets. Grbčić et al.[72] demonstrated an automated, high-throughput workflow using femtosecond laser processing producing over 11,000 metasurface samples in a single run. This captured both fabrication variability and measurement noise in their experimental dataset. The limitations on high-throughput, high-resolution, large-scale nanofabrication are a stumbling block that needs to be overcome to be able to obtain sufficient experimental data to robustly train the models. However, combining generative augmentation with automated experimental sampling has been proven to produce datasets that are sufficiently large and realistic to cover complex design variations, enabling inverse-design models to learn robust representations and generalize effectively to new, unseen metasurface geometries.

Despite the advances in AI-driven metasurface design, the practical realization of these designs remains constrained by fabrication limitations. Nanoscale devices, in particular, are subject to strict rules such as minimum feature sizes, aspect ratios, and tolerances in etching and deposition processes. Designs that neglect these constraints often fail, exhibiting low yield and poor reproducibility. Integrating fabrication-aware constraints directly into the design stage not only reduces wasted iterations but also increases the likelihood of experimental success[73–75]. Recent studies have proposed effective strategies to embed fabrication feasibility into the design process. For example, Zhou et al.[76] parameterized each meta-atom by width, length, displacement, and rotation, which are mapped through analytic and differentiable transformations to fabrication-compliant geometries. This parametrization ensures simple shapes with uniform feature sizes and low aspect ratios suitable for nanoscale fabrication, guiding optimization toward experimentally viable candidates while mitigating lithographic proximity and etch variability. Complementarily, Ueno et al.[77] combined a fast generator with a surrogate model under experimentally calibrated to minimum-size and gap rules, constructing a constraint-aware meta-atom library. A figure-of-merit selector preserves full 2π phase coverage while filtering designs that satisfy fabrication tolerances, enabling rapid system-level synthesis without exhaustive full-device simulations (Fig. 3(c)). While incorporating fabrication constraints nominally reduces the size of the design space, it strategically focuses exploration within physically realizable regions. This not only prevents unbuildable designs but also accelerates the discovery of high-performance metasurfaces that can be reliably fabricated, bridging the gap between computational optimization and practical implementation.

2.3.2 Practical deployment and application

2.3.2.1 Scalability and transferability

Large-scale metasurfaces are increasingly in demand for practical optical applications, where devices must cover centimeter-scale apertures. Designing such large-scale metasurfaces is challenging, and traditional approaches often rely on a locally periodic approximation, assuming weak coupling between neighboring meta-atoms to simplify the design[78]. While this assumption is generally valid, it breaks down when near-field interactions are required, or nonlocal effects become important. Consequently, full-device optimization becomes computationally demanding and difficult to scale. To address this, recent studies have proposed strategies that partition the metasurfaces and manage interactions

modularly[79]. For example, one approach adopts a panel-based strategy, dividing a centimeter-scale metasurface into panels, each handled by a dedicated network[80]. A coordinator assembles their responses into a complete device. This modular design allows reusing different sizes or layouts, and converts a large-scale optimization problem into several smaller, tractable subproblems. A complementary strategy[81] uses superpixel or patch-based optimization, dividing the surface into wavelength-scale patches that are optimized in parallel. Nonlocal interactions are incorporated at the patch level, ensuring that higher-order effects and multifunction targets remain coordinated after assembly. While this method favors parallel throughput and precise handling of inter-element interactions, it is sensitive to the fidelity of the interaction model and may require careful calibration to avoid residual mismatches across patches. Both approaches share a divide-and-conquer strategy but rely on different assumptions, making each suitable for distinct use cases. Panel-based inheritance is advantageous when rapid redesign and component reuse are prioritized, whereas patch-based optimization is preferable when parallel computation and strict coordination of interactions are critical. Overall, introducing explicit partitioning and coordination mechanisms enables scalable design of large metasurfaces while maintaining computational efficiency and global performance fidelity.

The predictive performance of inverse-design models for metasurfaces often deteriorates when applied beyond their training distribution, making transferability a critical consideration. Two practical scenarios illustrate this challenge: 1) extrapolation within the same physical regime and 2) adaptation across distinct spectral bands. In the first case, frequency extrapolation addresses the challenge of predicting spectral responses in a frequency range just beyond the training data, under the critical assumption that the underlying physical laws of the system remain unchanged. For instance, Zhu et al.[82] addressed this by combining multi-fidelity operator learning with a latent-dynamics model to propagate hidden states along the frequency axis, enabling accurate estimation beyond the training span (Fig. 3(d)). A hybrid-regularized inverse module further stabilizes design predictions under modest regime shifts. While effective within the same regime, accuracy can decline near newly emerging resonances.

Cross-band transfer presents a more demanding scenario, as spectral characteristics may differ significantly. Xu et al.[83] addressed this by pretraining a complex-valued network on infrared (IR) spectra and fine-tuning all layers on a small terahertz dataset. This approach preserves beneficial prior knowledge while allowing full adaptation to the target regime, achieving ~26% higher accuracy compared with training from scratch and ~30% lower error than real-valued baselines. Nevertheless, the effectiveness of transfer depends on the degree of similarity between source and target physics; changes in dispersion or the presence of bandgaps may limit applicability. In practice, frequency extrapolation is suitable for extending the predictive range of a model within a consistent physical framework. In contrast, cross-regime adaptation is essential when the goal is to leverage existing knowledge for a new application in a distinct spectral domain where the underlying physics may differ.

2.3.2.2 Interpretability and user-friendly AI

Most AI models operate as black boxes, offering little insight into the physical rationale behind design choices[63,84]. This lack of interpretability does not allow us to understand why a certain design choice is better than another, therefore explainable-AI (XAI) techniques have been increasingly adopted in metasurface design[85]. To explain the science and physics behind any decisions, XAI generally includes physical laws and relationships, such as PINNs. For instance, You et al.[86] integrated physical constraints directly into a semi-black-box network by embedding the Kramers–Kronig causality relations during training. This approach ensures that the network respects fundamental physical laws rather than simply fitting data, producing output spectra whose internal structures are physically consistent. Dimensionality-reduction using t-distributed stochastic neighbor embedding revealed that the networks learn physical patterns, enabling intuitive interpretations of which spectral features drive design decisions.

Visualization-based XAI methods further enhance interpretability. Gao et al.[65] employed attention-based mapping to identify key spectral features influencing the choices of the model. For example, high attention on resonance regions directly indicates the meta-atom geometries prioritized by the model, providing a clear connection between physical signals and design outcomes. Ensemble-based approaches offer complementary insights. Chen et al.[85] improved interpretability with random forests[87] where the explicit decision paths and probabilities allow quantitative assessment of design likelihoods and the relative importance of each structural parameter. This enables direct evaluation of which physical variables most strongly influence target performance. Collectively, such explainable and interpretable design methods expose AI-driven design decisions transparently, facilitating iterative optimization, and physical understanding and enabling a more informed metasurface design process.

Nanophotonic inverse design traditionally requires substantial physics expertise, careful simulation setup, objective formulation, and nontrivial coding and debugging, creating a high barrier to entry. User-friendly AI interfaces, particularly large language models (LLMs) offer a promising pathway to lower this barrier by translating natural-language requirements into design variables and executable code, thereby enabling faster prototyping and broader participation.

At the front-end, LLMs can serve as interactive assistants that translate user intent into specifications and computa-

tional routines. For example, Kim et al.[88] demonstrated that, with in-context examples, an LLM can generate transfer-matrix code, suggest objective functions and optimization strategies, and rapidly update candidate designs in response to user feedback. Such models can also propose multiple alternative designs for the same target, facilitating early-stage exploration and comparative evaluation (Fig. 3(e)). At the back-end, domain-specific generators can systematically translate specifications into fabrication-ready candidates. Ma et al.[89] introduced structure tokens and structure serialization, conditioning generation on a target spectrum to produce variable-length layer sequences. This approach allows process constraints to be incorporated directly into the generation pipeline while supporting the sampling of diverse, constraint-compliant candidates.

Despite these advances, the reliability of such models is an open question. Their knowledge is derived from broad, internet-scale text and code rather than curated expert systems, making them susceptible to hallucination, generating plausible but factually incorrect outputs. Furthermore, LLMs and generative frameworks often exhibit restricted explainability, dependence on large datasets, and expressivity constraints from discretized materials and thicknesses. Consequently, verification, iterative feedback, and explicit incorporation of fabrication constraints are essential to ensure reliability and reproducibility. Integrating front-end conversational assistant LLMs with back-end constraint-aware generators can establish a workflow that is both accessible and physically grounded. By reducing reliance on specialized expertise, accelerating early prototyping and maintaining design fidelity, such user-friendly AI interfaces may open up metasurface design to a wider audience and broaden participation in metaphotonic engineering.

3 AI for characterization and analysis of metasurface optical outputs

Metasurfaces can freely manipulate the multidimensional properties of light, producing optical data such as reflectance, transmittance, scattering, and absorption spectra, as well as 2D images that capture light-matter interactions. Yet, conventional physics-based or empirical methods often fall short in capturing the nonlinear, noisy, and multi-dimensional features of fabricated metasurface spectra. Artificial intelligence, and deep learning in particular, provides a compelling alternative by uncovering hidden patterns and correlations that conventional approaches cannot resolve. Since DNNs have demonstrated strong capabilities in uncovering subtle relationships between input and output data, they are a powerful tool for uncovering hidden patterns within optical data, enabling advanced AI-driven measurements and sensing in metasurface-based systems[90,91]. This section introduces the recent progress in AI-driven evaluation and analysis of metaphotonic systems or applications such as optical data storage, biosensing, and imaging.

3.1 Advanced spectral analysis and sensing system

Even in their simplest form, one-dimensional (1D) spectral data contains rich wavelength-dependent information about light-matter interactions. Peaks, troughs, and line shapes reveal resonances that serve as optical fingerprints, while quantities such as loss rates and *Q*-factors provide sensitive evidence for subtle changes in the optical environment. Such resonance-based measurements have been utilized extensively in numerous sensors[92], and rely on a high *Q*-factor resonance to provide high resolution. In practice, however, metasurface responses often involve multiple overlapping resonances, modal interference, and other intricate physical effects, resulting in highly nonlinear and complex spectral patterns. Such characteristics make it challenging for traditional physics-based models or empirical analysis methods to fully explain or generalize the observed responses. Consequently, AI models have been increasingly introduced into data-driven spectral analysis, enabling the learning of nonlinear patterns, multivariable correlations, and high-dimensional representations embedded in spectral data, and thereby providing physical insights and facilitating the analysis of complex optical responses that are difficult to capture with conventional approaches.

3.1.1 1D spectral analysis and application

Leveraging these properties, 1D spectral analysis has found broad applications, particularly in optical storage and diverse sensing platforms. When analyzing 1D spectral data, models such as 1D CNNs and fully connected DNNs have been commonly used. These models offer the advantage of capturing both local features and global patterns within the spectrum and have been widely applied to various tasks, including classification and regression. Analyzing these spectra enables the decoding of subtle structural variations and the classification of optical states, making it essential for applications such as high-density optical storage. Wiecha et al.[93] demonstrated that DNNs can learn complex relationships between 1D scattering spectra and the geometric configurations of silicon meta-atoms, achieving 9-bit information decoding with up to 40% higher density than conventional Blu-ray storage. This work highlights the power of implementing AI in the analysis and evaluation of metaphotonic structures for optical data storage, which could lead to ultrahigh capacity physical storage devices.

In addition to optical storage classification, the analysis of 1D spectral data from metasurfaces using AI has also been applied to biosensing systems by automatically detecting shifts or changes in resonance peaks. Spectral features observed in spectrum data, such as resonance peak shifts and variations in transmittance or reflectance intensity, respond sensitively to external environmental changes or

material composition. Such spectral features have been widely exploited in various sensing applications, including biosensing[94,95], gas detection[96,97], and chemical classification[98] (Fig. 4(a)). For instance, Wekalao et al.[99] utilized resonance peak shifts to detect changes in refractive index, applying this principle to develop a biosensor capable of monitoring variations in biomolecular concentrations. In their plasmonic resonance metasurfaces, changes in hemoglobin concentration lead to refractive index variations in blood samples, which in turn induce shifts in the resonance peaks of the transmission and reflection spectra. By applying refractive index changes corresponding to hemoglobin concentrations ranging from 10 g/L to 40 g/L, the performance of the sensor demonstrated a sensitivity of 3500 nm/RIU (refractive index unit) in the IR range. An AI model was trained to accurately predict the transmission response based on various sensor geometries, the chemical potential of graphene, and changes in the refractive index. Based on spectrum response vectors proportional to transmittance, Meng et al.[96] proposed a compact and portable gas sensing system operating in the mid-IR (7–14 μm) range (Fig. 4(b)). This system integrates a multi-channel metasurface spectral filter array with a microbolometer camera. The metasurface consists of 20 independent filter channels, each providing distinct spectral responses to extract transmittance information from IR light that has passed through a gas sample, enabling the system to capture the unique mid-IR "fingerprints" of various gases. The labeled data was trained using a support vector machine algorithm, enabling rapid and accurate gas identification directly from the sensor output without complex spectral reconstruction, achieving a high accuracy of 94.4% for methyl ethyl ketone detection. Despite these successes, 1D spectral data inherently represent a single wavelength-dependent output vector, which limits their ability to capture multi-dimensional physical effects such as polarization, modal interactions, incident angle variations, and spatial dependencies. This limitation becomes particularly critical for multifunctional metasurfaces, where complex design degrees of freedom and changes in external stimuli (e.g., changes in refractive index, chemical composition, or temperature) induce layered responses. As a result, a single spectrum is often insufficient to fully interpret or distinguish these intricate characteristics.

3.1.2 Multi-dimensional spectral data and application

The multifunctionality of metasurfaces enables additional degrees of freedom in the optical response, making multi-dimensional spectral analysis increasingly important to capture the interplay of multiple physical parameters. However, such multi-dimensional spectra inherently involve

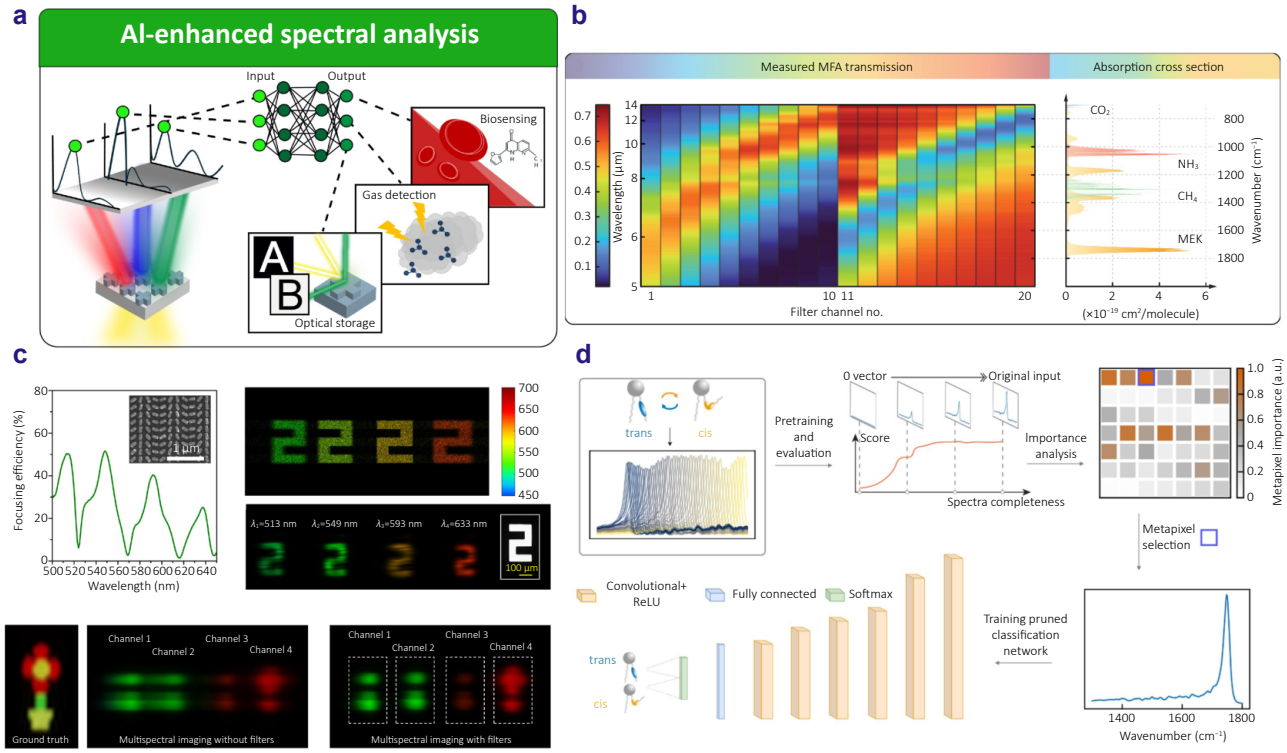

Fig. 4 | AI-assisted analysis of spectral data. (a) Schematic figure of AI-based analysis of spectral data manipulated by metasurfaces. (b) Visualization of readout data and temperature stability. (c) The measured focusing efficiency and the 4-band multispectral images, acquired both computationally and experimentally, demonstrate snapshot multispectral imaging without the need for filters. (d) Feature extraction framework and classification model of XAI. Figure reproduced with permission from: (b) ref. [96], (c) ref. [104], (d) ref. [105], under a Creative Commons Attribution License.

intricate interactions and high-order nonlinearities among variables, which often exceed the capabilities of conventional analysis methods. This calls for AI-based evaluation tools that provide insights beyond what simple analytic models can provide[100,101]. For example, Herpin et al.[102] proposed a surface-enhanced IR absorption spectroscopy sensor using a broadband IR nanoplasmonic platform combined with AI to monitor dynamic molecular interactions in vivo without the need for labels and in real time. DNNs were adopted to mitigate the limitations of conventional multiple linear regression, including spurious signals from uninjected molecules, interference caused by water, and diffraction artifacts. Trained on millions of real-time spatiotemporal spectral data points, the DNN was able to autonomously capture distinctive patterns and complex nonlinear relationships. This allowed the successful detection of dual cargoes (sucrose and nucleotides) release from perforated liposomal membranes and enabled monitoring of supported lipid bilayer formation, significantly improving both sensor performance and analytical reliability. Similarly, Yang et al.[103] proposed a novel platform combining large-area spatially gradient metasurface with AI for simultaneous classification and concentration prediction of small molecules in solution. The transmittance patterns of the metasurface sensitively respond to changes in the refractive index of the surrounding environment, effectively encoding molecular species and concentration. CNN was utilized to analyze these transmittance patterns, leveraging tailored loss functions and positional information of sensitive areas on the metasurface to enhance learning efficiency and concentration prediction accuracy. Experimental results demonstrated high accuracy in predicting molecular concentration with an average error of 10% for a true concentration of 10% and reliably distinguished three different molecules (glycerol, glucose, and sucrose) in mixed solutions, demonstrating its capability for robust molecular classification and quantification.

Hyperspectral imaging (HSI) has emerged as a powerful technique for acquiring both spectrally and spatially resolved multi-dimensional spectral data, enabling more comprehensive analysis of material composition and dynamic interactions. This makes it possible to analyze subtle chemical and physical differences that are imperceptible to the human eye, and to accurately detect the presence of specific substances[106,107]. However, conventional HSI systems often rely on bulky optical components and multi-shot acquisition processes, resulting in large and burdensome setups. To overcome these limitations, recent approaches have explored the integration of compact and lightweight metasurfaces with AI-driven fast data processing[108]. For example, Makarenko et al.[109] proposed a compact real-time HSI system that combines a metasurface-based hardware spectral encoder with an AI-powered software decoder. Each metapixel of the metasurface, placed directly atop a standard image sensor, is designed with a unique spectral response function, converting the high-dimensional spectral data into a low-dimensional "barcode" of nine intensity values. The compressed barcode data are decoded using a multilayer perceptron for spectral reconstruction, while a U-Net architecture is applied for semantic segmentation tasks. Experimental results demonstrated that this real-time HSI system outperforms conventional RGB-based models, achieving a mean intersection over union of 81% in simulation and 74% in real-world experiments, compared to 68% for the RGB baseline, highlighting its enhanced hyperspectral feature recognition capability. Similarly, Lin et al.[104] developed an ultra-compact snapshot HSI system based on a single multi-wavelength metasurface chip, capable of capturing 4-band multispectral images in a single acquisition and reconstructing an 18-band hyperspectral data cube using deep learning (Fig. 4(c)). Optical aberrations induced by the metasurface are computationally corrected through a transformer network, while a CNN is trained to learn the complex mapping between the 4-band input and the 18-band target spectrum. The reconstructed hyperspectral data exhibits low mean squared error compared to the ground truth, low root mean squared error and spectral angle mapper values, confirming its high fidelity.

3.1.3 Dimensionality reduction and interpretability in spectral analysis

As spectral data often exhibit complex and optically overlapping properties, compressing them into a lower-dimensional representation can be an effective approach for streamlined analysis and computational efficiency. This dimensionality reduction facilitates the separation of key underlying physical properties embedded within the spectra, thereby improving the stability and performance of subsequent machine learning models[110,111]. Ren et al.[112] proposed an analytical framework that interprets high-dimensional spectral measurements as multi-dimensional sensing inputs, enabling systematic decomposition and classification. Mid-IR spectra were compressed into a compact feature space using principal component analysis, successfully disentangling distinct physical phenomena such as refractive index variation, molecular absorption, and resonance mismatch along independent analytical axes. These extracted features were then used to train a support vector machine, achieving 100% accuracy in distinguishing chemically similar alcohol mixtures. This study highlights the potential of machine learning for interpreting complex spectral information and enabling high-precision molecular recognition. Nonetheless, most AI models remain black boxes, emphasizing the ongoing need for approaches that provide outputs interpretable by humans.

To address this, recent studies have integrated XAI techniques into spectral analysis. XAI enables quantitative interpretation of the physical correlations between structure parameters and spectral responses and visually identifies which structural features most influenced specific wave-

length bands[113]. Such methods allow systematic sensitivity analysis of structure parameters, evaluation of wavelength-specific impacts, and structure–response correlation analysis. Barkey et al.[105] applied this strategy to detect subtle spectral changes in complex molecular systems under dry conditions. Using a 1D CNN trained on extensive spectral data obtained from pixelated metasurfaces, they classified *cis*- and *trans*- lipid membrane states with high accuracy, and XAI techniques subsequently identified the key spectral regions driving the decisions (Fig. 4(d)) revealing that structural changes induced by the photoisomerization process in lipid membranes were sensitively reflected in specific vibrational modes, and critical for classification. In this way, XAI and other AI techniques are proving to be effective tools for complementing conventional analysis methods by providing quantitative, interpretable insights into high-dimensional spectral data.

The research introduced in this section demonstrated the potential of 1D and multi-dimensional spectral analysis combined with AI for high-precision sensing and interpretation. From resonance-based biosensing to HSI and neural network-based classification, AI-based analysis has shown strong capabilities in decoding complex spectral patterns and uncovering meaningful physical relationships, particularly in cases involving nonlinearities, noise, or overlapping features. Such research has an extremely important role to play in biophotonics and biomedical applications, where metasurfaces could be integrated into flexible or wearable devices with onboard lightweight AI systems, as well as in providing a lightweight solution for hyperspectral imaging, which could revolutionize drone-based monitoring and defect recognition.

3.2 AI-enhanced imaging in metasurface systems

Metasurface imaging systems that utilize 2D image data can readily acquire information using standard sensors such as charge-coupled devices, since images are direct and intuitive representations of optical responses. Compared to 1D spectral data that require expert knowledge and complex acquisition setups, 2D images provide an easier and more accessible pathway for data collection and analysis, which makes them particularly valuable for practical applications. Furthermore, metasurface-based imaging systems offer additional advantages in terms of miniaturization, integration, and multifunctionality. Metalenses in particular provide a direct way to create a metasurface-based imaging system. These characteristics make them particularly attractive for next generation compact and wearable optics, such as augmented reality (AR) and virtual reality (VR) devices[114]. However, metalenses are inherently affected by aberrations, limited by image sharpness, contrast, and signal-to-noise ratio, thereby limiting resolution, field of view (FOV), and overall fidelity in practical applications. To address these challenges, recent studies have focused on applying AI-based enhancement and restoration techniques to metasurface imaging systems[115]. Furthermore, AI has been implemented to extract additional dimensionality from simple 2D data, such as depth and phase information (Fig. 5(a)).

Chromatic aberration is one of the inherent difficulties for single layer metasurfaces due to the wavelength dependent nature of beam steering and material dispersion. Through the application of AI, this has been successfully corrected, leading to significant improvements in image quality through perceptual loss minimization and peak signal-to-noise ratio (PSNR) optimization[116]. Dong et al.[117] employed a U-Net architecture to correct chromatic aberration in images captured with a single chromatic metalens. The model, trained on a diverse dataset of objects, colors, and brightness levels, minimized both perceptual and PSNR losses, achieving a 5.5 dB increase in PSNR and over 12% improvement in structural similarity index measure (SSIM), demonstrating a substantial enhancement in image quality. Similarly, Chu et al.[118] developed a GAN-based deep learning framework with a U-Net generator and attention mechanisms, optimizing perceptual and color loss through iterative adversarial learning. The model demonstrated significant improvements in image restoration, roughly doubling PSNR and increasing SSIM by over 0.7 compared to autoencoder-based and standard U-Net methods (Fig. 5(b)). Its performance was robust across datasets of varying complexity, effectively correcting dispersion-induced distortions and successfully restoring visual clarity. These results highlight the potential of AI-enhanced metalens imaging for high-fidelity image reconstruction in practical applications.

Outside of overcoming chromatic aberration, challenges including limited FOV and full-color image reconstruction have been addressed with AI-enhanced metalens systems. These approaches aim to improve visual fidelity by extending spatial information and correcting spectral inconsistencies across color channels[119–121]. Chen et al.[119] implemented a computational image reinforcement approach to achieve a wide FOV in compact augmented reality (AR) devices, which are essential for miniaturization. They achieved a wide FOV of 30° with total distortion suppressed to below 2%, and maintained a relative illumination above 0.9 across the entire FOV. Beyond FOV expansion, Liu et al.[121] integrated an ultra-wide FOV meta-camera with a transformer-based neural network, achieving full-color imaging with an FOV exceeding 100° while correcting chromatic aberrations and distortions. The network, pre-trained on simulated point spread functions (PSF) and fine-tuned with real measured data, demonstrated 13.5-fold and 2.7-fold contrast improvements in central and edge regions, respectively (Fig. 5(c)). Furthermore, the metalens achieved a resolution close to the diffraction limit of 1.55 μm at the image center. Consistent image reconstruction quality was also observed in real-world environments at various working distances (e.g., 1.3 cm, 12 cm, 44.5 cm), with its quantitative excellence confirmed by PSNR and SSIM values. Supported by

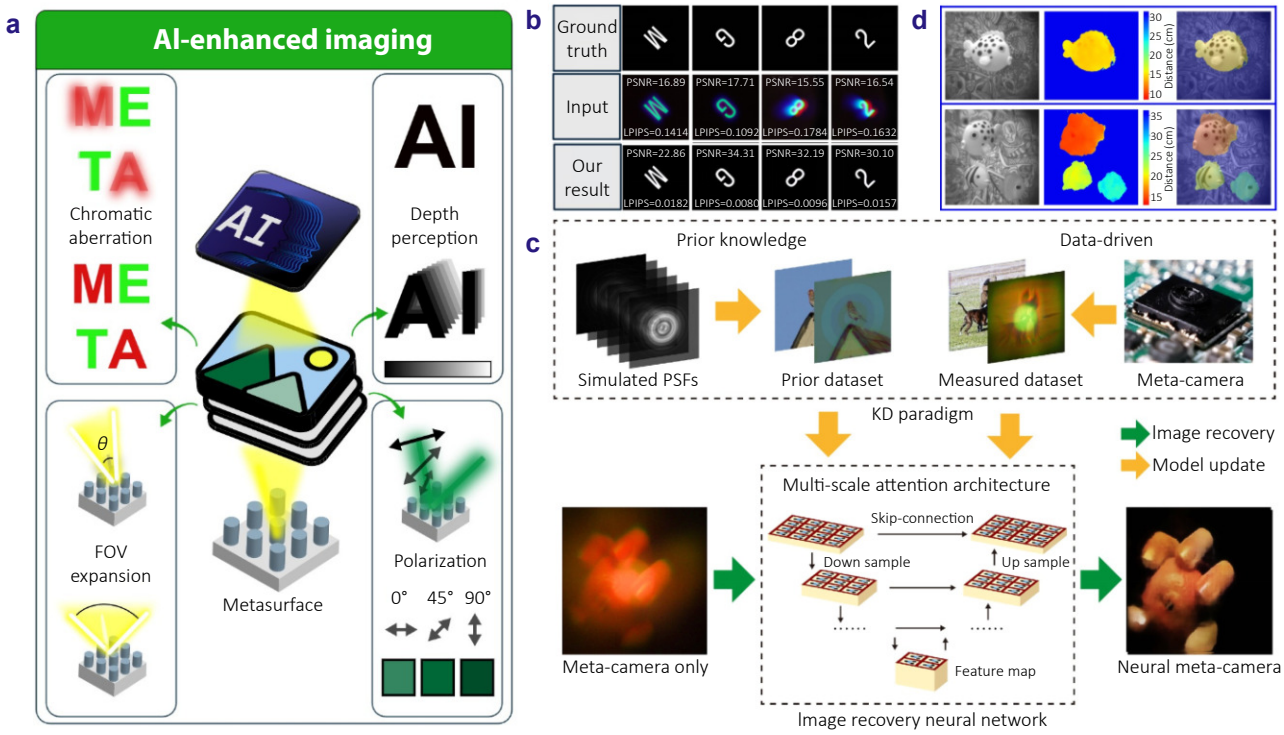

Fig. 5 | AI-enhanced metaphotonic imaging. (a) Schematic figure of AI-enhancement of metaphotonic imaging systems. (b) Comparison of ground truth images, input images affected by chromatic aberration, and restored outputs from the autoencoder, standard U-Net, and GAN-based framework. (c) Neural meta-camera model process to enhance image quality. (d) Underwater depth-sensing results using image data from a binocular metalens, showing the raw images, depth maps, and integrated outputs. Figure reproduced with permission from: (b) ref.[118], (c) ref.[121], (d) ref.[130], under a Creative Commons Attribution License.

large-scale nanoimprint fabrication[122], Seo et al.[123] achieved aberration-free full-color imaging with mass-produced metalenses. The highly chromatic and angular aberrated 10 mm diameter metalens was used to collect around 700 ground truth images from a large monitor for network training. The resulting images from the AI-enhanced metalens framework were restored to be comparable to the ground truth and further demonstrated their applicability for object detection. Combining the benefits of AI to combat the weaknesses in metalens-based imaging has been shown to be a powerful tool in AI-enhanced metaphotonic systems.

High-resolution color restoration that enables the recovery of fine structural details is also essential for the practical implementation of metalens imaging. Zhang et al.[124] proposed a digital imaging system that combines an RGB achromatic metalens employing spatial multiplexing with a neural network–based restoration framework. Although the metalens achieved a high numerical aperture (NA) of 0.97 and a spatial resolution of 0.775 μm for each RGB channel, the spatial multiplexing strategy introduced image blurring due to variations in the PSF and modulation transfer function across channels. To mitigate this issue, a computational restoration algorithm based on a neural network was incorporated. The network was trained to minimize the loss between blurred images captured by the metalens and their corresponding ground truth images. Multi-scale SSIM loss was used to preserve high-frequency contrast, while the mean absolute error minimized the absolute difference in pixel values between the restored and ground truth images, ensuring accurate color and brightness restoration. As a result, the processed images showed significant improvements in color fidelity and sharpness, with image blurring greatly reduced. The system also demonstrated fast inference performance, achieving an average processing time of 84 ms per image.

Recent AI-enhanced metasurface imaging systems are also increasingly exploring the rich, multidimensions of optical properties by leveraging the unique image information provided by metalens. Metalens-based imaging systems inherently encode complex phase, polarization, and depth-related information, and AI provides an optimal framework to decode and leverage these multidimensional features[125–128]. For example, Yang et al.[129] proposed a deep-learning-based colorimetric polarization-angle detection method utilizing asymmetric all-dielectric metasurfaces. The metasurfaces achieve high monochromaticity and a wide color gamut, generating dual-color palettes with abundant combinations depending on the incident polarization. By systematically varying the polarization state in 0.05° increments, they acquired color palette images for a total of 1801

polarization angles and under three different illuminant conditions, thereby building an extensive dataset. This collected image data was then used to train a polarization detection network. The model was trained to classify polarization angles into 129 classes and achieved 81.4% accuracy on the test dataset. In addition, research has actively explored the extraction of new information, such as depth, from metalens-based imaging systems, with learning-based models playing a central role in this process. Liu et al.[130] developed a binocular metalens-based depth sensing and imaging system that requires neither distortion correction nor camera calibration. Their GaN-based metalens, featuring superhydrophobic properties, enabled high-quality stereo imaging in underwater environments without additional optical adjustments. The captured stereo images were processed by a trained deep learning model which learned to compute subtle pixel-level disparities between image pairs. This allowed the system to generate precise real-time disparity maps for each pixel. Ultimately, the model achieved depth estimation within an error range of 50 μm and enabled real-time underwater depth sensing in just 0.15 seconds without any manual parameter tuning (Fig. 5(d)).

Recent advances in AI-enhanced metasurface imaging have focused on overcoming chromatic aberration, narrow FOV, and reduced spatial resolution, leading to substantial improvements in overall image fidelity. Rather than extracting new physical quantities, these approaches predominantly aim to restore image quality and compensate for dispersion-induced distortions, thereby enhancing the practical viability of metasurface-based imaging systems. Unlike spectral data, metasurface-based image data faces several constraints, including the difficulty of obtaining reliable ground truth, limited information density, and high costs associated with data acquisition. To overcome these limitations, recent studies have explored learning strategies that can effectively utilize small datasets, as well as integrated approaches that combine AI with hardware sensors[131]. Collectively, these efforts highlight the importance of co-designing hardware and algorithms to optimize both physical and computational resources, enabling metasurface imaging systems to move closer to practical deployment.

4 AI-driven end-to-end metasurface systems

While AI has been utilized in metaphotonic research separately for the inverse design and for characterization of optical outputs from metasurface-based systems, these approaches create a disconnect between the ideal designs and fabricated devices. On the other hand, by creating a differentiable pipeline between the design and characterization directly, it is possible to create end-to-end systems that can be optimized with consideration of the fabrication constraints and complete physical systems. We note here that the term 'end-to-end' has also been used in the metasurface community when discussing the training of forward and inverse DNN models in tandem[73]. However, in this review we focus specifically on the recent development of metaphotonic systems with co-optimized design for the metasurface hardware alongside the computational backend for characterization and analysis.

4.1 Co-optimized metasurface design

By moving away from the inverse design of meta-atoms and metasurfaces, system-level end-to-end optimization with fully differentiable pipelines is establishing a new paradigm of the application of AI in metaphotonic systems. This approach creates a multivariable objective, from metasurface inverse design to practical application, such as high-resolution imaging, depth sensing, or polarization reconstruction (Fig. 6(a)). This process exists for traditional optics[132], and is now being implemented into metaphotonic systems. Rather than the traditional method of designing meta-atoms to fulfill a specific phase profile, resulting in mismatches due to physical limitations of materials and fabrication, end-to-end optimization allows the realizable phase, free-space propagation, and sensor response to be simultaneously considered. This integration has led to advanced imaging systems with metaphotonics for holography, as well as super-resolution and 3D imaging, shifting metasurface design from physical-response maximization to task-oriented optimization with goals such as accuracy, perceptual quality, and real-world deployability.

Metalenses have developed from single functionality, single wavelength demonstrations of feasibility to current state-of-the-art flat optical imaging devices that demonstrate high-NA, achromatic, and multifunctional operations[133–135]. However, single layer metalenses suffer from a reduction in imaging quality due to various aberrations, limiting their use in real-world imaging systems. To solve this issue, not only is research being conducted on post-processing image correction using AI, but an innovative approach called end-to-end design is also gaining attention. This method considers the phase of the metalens, the propagation of light, and the sensor response within a single, integrated pipeline. This allows for the design of a lens that anticipates and compensates for the constraints and aberrations that may arise during the fabrication process from the very beginning. Through this AI-based end-to-end optimization, researchers have been able to fundamentally mitigate aberrations and successfully generate high-quality, full-color images even with a wide FOV, significantly enhancing the performance of metalenses. In one example, Tseng et al.[136] included a proxy function of their metalens, based on the scattering of individual meta-atoms, to simulate the PSF including the inherent noise from the sensor. The proxy function allows for gradients to flow through the whole

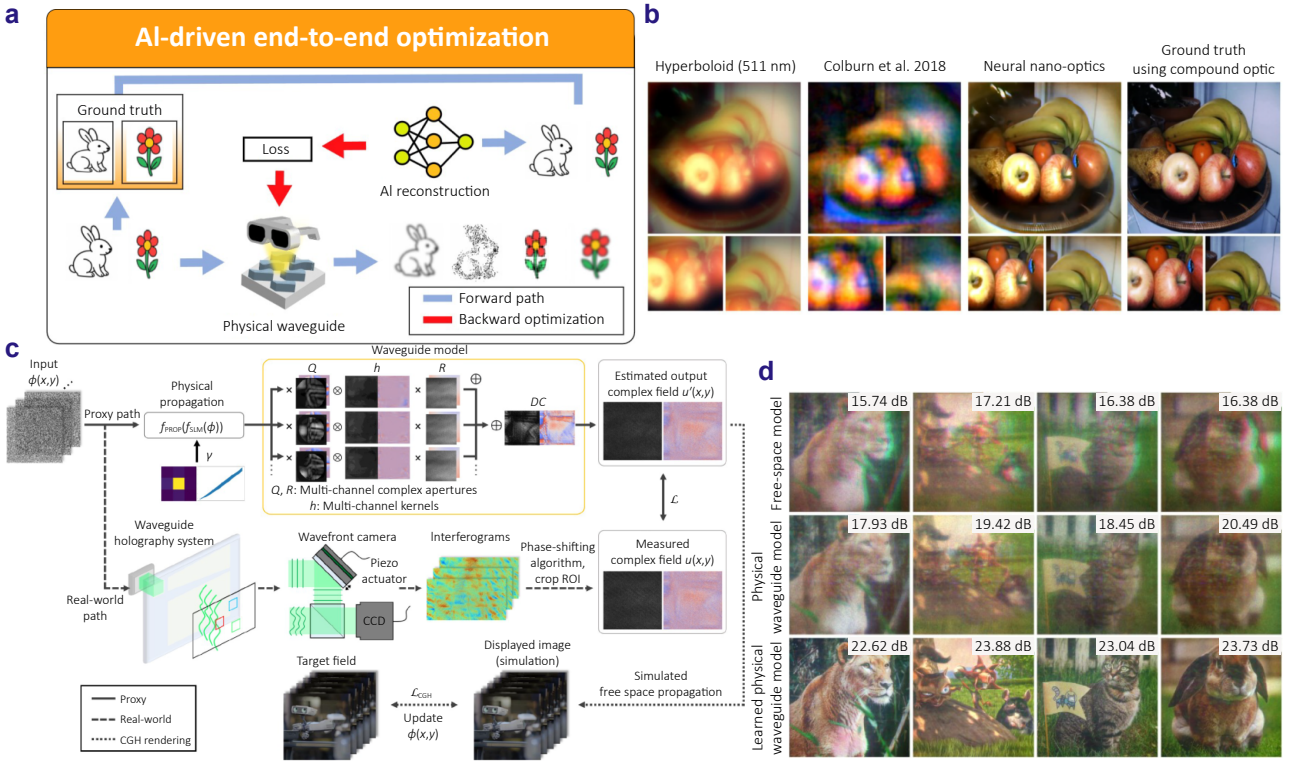

Fig. 6 | AI-driven end-to-end optimization. (a) Schematic illustration of the end-to-end optimized metasurface pipeline. (b) The end-to-end designed neural nano-optics produces high-quality, aberration-free, wide FOV images. (c) An end-to-end pipeline for complex wavefront measurement-based model calibration and optimized computer-generated hologram rendering in a waveguide holography system. (d) Comparison of 2D holograms synthesized using several different wave propagation models, including free-space propagation, a physically motivated model and AI-powered model including physics and learnable parameters that are calibrated using camera feedback. Figure reproduced with permission from: (b) ref.[136], (c) ref.[146] (d) ref.[145], under a Creative Commons Attribution License.

system, enabling the use of automatic differentiation. This step is extremely important, as the standard process of selecting meta-atoms to fulfill a phase mask would eliminate all gradients at the metasurface. Additionally, this approximation is much faster and memory efficient compared to full-wave simulations such as FDTD. The final AI-enhanced metalens imaging system provides real-time frame rates with performance that is comparable to traditional six-element compound optics (Fig. 6(b)). Pinilla et al.[137] replaced the numerical modelling of the PSF by implementing a spatial light modulator to mimic the role of the metasurface, allowing for computation-free iteration and updates of the required phase profile. After the optimization process, the phase mask was replaced with a single metasurface to demonstrate ultra-thin full-color imaging cameras. Park et al.[138] included an aperture stop in their metalens system to alleviate off-axis aberrations such as coma and astigmatism for a 70° FOV. By fabricating the aperture stop on the opposite side of the metalens substrate to create a doublet system, and employing end-to-end optimization of the metalens phase and reconstruction algorithm full color imaging was successfully demonstrated. A challenge for achromatic imaging with metalenses is the limitation of physical size, particularly the diameter. Fröch et al.[139] showed a 1 cm diameter metalens with imaging performance comparable to a single refractive lens through their end-to-end design and optimization process. Rotational symmetry was exploited to reduce computational expense, and a beam splitter was used to collect one-to-one pairs of images from the metalens and a compound lens for training. Furthermore, the multispectral capabilities of metasurfaces have been exploited for designing metalenses that operate at IR wavelengths, specifically for imaging of thermal radiation[140].

While metalenses focus on imaging, metasurface-based holography, known as metaholography, is a field that creates images through that manipulation of the phase and amplitude of light. Traditionally, iterative algorithms such as the Gerchberg–Saxton algorithm are used for phase retrieval, and meta-atoms are designed to fit the required phase map. AI-based methods have also been proposed for phase retrieval, for example using gradient descent[10] and physics-driven DNNs[141]. However, with end-to-end optimization, direct meta-atom selection based on material, and geometric parameters can be directly optimized[142], and additional

noise and imperfections from light propagation and sensor readout, can be integrated into the process. While the multiplexing nature of metasurfaces naturally allows for multichannel holography, providing a path towards multi-dimensional holography, the design of such metasurface becomes burdensome. Yin et al.[143] demonstrated an AI-powered pipeline to create metaholography with amplitude, phase, wavelength, and polarization dependencies. Using meta-atoms with only 2 degrees of freedom, they showed holographic displays with up to 12 channels, including 3 wavelengths, 2 polarization states, and two reconstruction planes. The scalar diffraction kernel is general and could be adapted based on the requirements of the system. The only limitation is that the kernel must be fully differentiable, which is easily achieved through machine learning packages such as PyTorch. Furthermore, Liu et al.[144] moved multiplexed metaholography from free-space to on-chip. By exploiting the properties of geometric and detour phase, they use end-to-end optimization to integrate a Si metasurface onto a Si_3N_4 waveguide. Different holograms appear based on the direction that the light is travelling inside the waveguide. This idea has been pushed further to create on-chip metaholography with up to 18 channels. Finally, waveguide-based holographic displays could play a key role in the future of AR devices, allowing for 3D image construction over a large eyebox. Gopakumar et al.[145] used the co-design of a metasurface waveguide and AI-based holography to create a full-color 3D holographic AR display system with AI trained using data obtained from both the physical metasurface waveguide and camera feedback (Fig. 6(c)). This system was developed further to create mixed reality displays with a large etendue and high image quality, across an eyebox of 98 mm[146], demonstrating that the mismatch between ideal properties in the system, such as the spatial light modulator, aberrations, and coherence of the source, can be effectively understood and corrected by a well-trained AI model. Finally, Jang et al.[147] demonstrated this with a modeling pipeline that includes both a computationally propagated path and a real-world path through the experimentally fabricated waveguide (Fig. 6(d)).

One of the most exciting potentials of AI-enhanced metasurface systems is to exploit multiple degrees of freedom of light for additional functionality. For example, by exploiting the wavelength as an additional degree of freedom, spectral and HSI becomes feasible. For instance, Lin et al.[148] realized multi-channel imagers reaching up to 16 distinct channels. They demonstrated multiwavelength spectral imaging, multi-depth imaging, and polarization imaging with the same framework. The strong dispersion of metalenses is often a drawback, however it has also been used as a way to distinguish spectral information. In work by Zhang et al.[149] HSI was demonstrated through an end-to-end optimized metasurface design and image processing method, outperforming separate optimization methods applied sequentially. This robustness was also demonstrated by Lin et al.[150] when they used full wave equation solvers in their design process to utilize all available wave physics to recover both spectral and polarization information. This would not be available with simple geometric optics and scalar diffraction.

Another advantage of metasurfaces is that depth information can be recovered from single-shot images, an application has broad potential in robotics, autonomous driving, and computer vision. With end-to-end optimization of the metasurface and reconstruction, a single-shot monocular metasurface camera combining RGB and depth imaging was achieved[151]. The optimization process took around 20 h on a consumer GPU, and allowed for an imaging depth range of 0.5 m. Another solution to depth imaging is to structure light to create point clouds of dot or line patterns[152]. Choi et al.[153] employed an end-to-end process to learn not only the optimized metasurface design, but also simultaneously the structured light pattern and reconstruction model. The full-space wave propagation over a 360° area, image formation, and reconstruction steps were all included into the optimization process and resulted in a depth reconstruction exhibiting a fivefold reduction in RMSE compared to heuristically designed structured light.

While end-to-end optimization of metasurfaces and their corresponding computational analysis is proving to be a valuable tool in the design of metaphotonic systems, it is important to note that the computational cost of such end-to-end systems becomes rapidly larger as device dimensions increase. Therefore, taking advantage of physics through symmetry, or the development of novel AI implementations could hold the key to facilitating deployable metaphotonic systems in the real world.

4.2 Intelligent metaphotonic systems

Passive metasurfaces have proven their ability to control light at the subwavelength scale, however, to unlock the full potential of metasurfaces with autonomous functionality, their optical properties must be controllable after fabrication[154,155]. Alongside integration with AI, such systems integrate real-time sensing, adaptive control, intelligent decision-making, and closed-loop feedback into a unified framework, enabling self-optimization in response to dynamic environments without human intervention (Fig. 7(a)). This section discusses the recent advancements in such autonomous metaphotonic systems for intelligent cloaking, sensing and communications, and biophotonic applications.

Since the advent of metamaterials, one of the first exotic applications that caught the attention of researchers was in invisibility cloaking[156]. The complete control of electromagnetic waves allows light to be directed around an object, rendering it invisible to an observer. By integrating AI with programmable metasurfaces, Qian et al.[157] demonstrated a microwave-frequency metasurface cloak capable of autonomously adapting to its environment on millisecond timescales. Here, a trained DNN acts as the brain of the

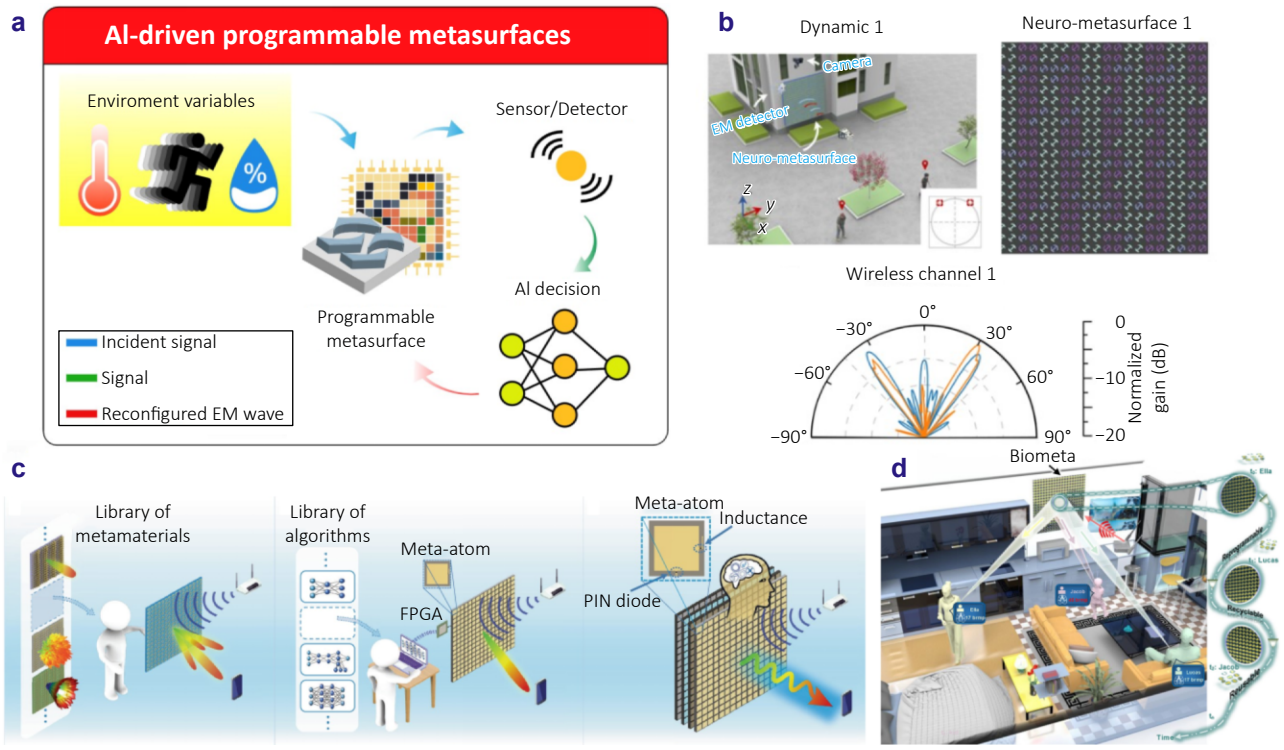

Fig. 7 | AI-powered autonomous metaphotonic systems. (a) Schematic illustration of autonomous metaphotonic systems. (b) Homeostatic/self-acting neuro-metasurfaces to enhance outdoor signals at the desired receivers or destructively at the non-intended receivers. (c) Paradigm shift of metamaterials, evolving from passive electromagnetic wave control devices to autonomous meta-agents capable of self-perception, reasoning, and action, thereby transcending human-directed functionalities. (d) Schematic illustration of the modular and reprogrammable BioMeta system for accurate non-invasive multi-person respiration monitoring with effective suppression of motion-induced noise. Figure reproduced with permission from: (b) ref.[161], (c) ref.[170] (d) ref.[174], under a Creative Commons Attribution License.

system, continuously updating the metasurfaces properties in real-time, creating a fully autonomous loop of perception, decision, and execution. Further advancements have expanded the operational versatility of intelligent cloaking. Zhen et al.[158] showed that transmission mode metasurfaces can be used for cloaking. To move this intelligent cloak into real-world scenarios, Wang et al.[159] developed full-polarization reconfigurable metasurfaces with thousand-level modulation, enabling high-fidelity background scattering matching of up to 93.3% even for moving objects and dynamically changing backgrounds. Finally, recognizing the practical limitation that cloaking inherently prevents electromagnetic interactions with the environment, Wang et al.[160] designed a metasurface cloak with switchable transparency, allowing the system to alternate between invisible and communicative modes. This innovation enables real-time information exchange between cloaked objects and external observers without compromising stealth, highlighting the potential for AI-driven metasurface platforms in next-generation adaptive cloaking and dynamic electromagnetic control.

The integration of AI with reconfigurable metasurfaces has opened transformative opportunities in wireless communications and radar sensing. Fan et al.[161] demonstrated homeostasis-inspired metasurfaces, wherein an AI-driven self-regulating reconfigurable metasurface system autonomously manages wireless channels. Such systems have potential disruptive use in electromagnetically connected smart cities (Fig. 7(b)). Intelligent metasurfaces have also been extensively explored for radar and beamforming applications, where real time steering and control of electromagnetic waves are critical[162,163]. Ma et al.[164] demonstrated that an array of reconfigurable dipoles can generate far-field patterns on demand. By integrating their reconfigurable metasurfaces with AI, combined with physics-based confirmation, they showed the potential for real-time metasurface beam-steering. Space-time-coding metasurfaces further extend this functionality by manipulating the optical properties of the metasurface in both the spatial and time domains[165], allowing for the generation of chirp signals and dechirp processing. This has been applied to a simplified radar architecture based on metasurfaces, with performance comparable to conventional systems[166], simultaneously supporting high-order harmonics generation for interference-free sensing, all within a single metasurface[167]. AI algorithms outside of fully connected DNNs have also been employed. Reinforcement learning has been applied to learn

the optimal control strategy through a simulated environment and to solve the joint optimization problem of beamforming and mapping of the received signals for object detection[168,169], and inspired by reasoning models in LLMs, metamaterial agents have been proposed[170]. The optical intelligent agent is a system that merges digital optics technology with AI to perceive the environment and autonomously control optical systems. It holds the potential to achieve outstanding performance in complex and variable environments, thereby moving beyond the limitations of conventional optics[171]. The agent can take multiple inputs, such as voice, image, and text that make up the environmental cues to make long-term plans that involve interactions with robots and humans to achieve a goal (Fig. 7(c)). With reasoning in natural language and multiple expert agents, this fully automated system demonstrates the potential of AI-powered metasurface platforms.

Outside of communications, AI-driven programmable metasurfaces have demonstrated significant potential in biophotonics, particularly for non-invasive monitoring. Their advanced sensing capabilities of metasurfaces allow detection of subtle changes in electromagnetic signals arising from biological and physical processes. For instance, Ma et al.[172] showed that programmable metasurfaces with well-trained DNNs can achieve recognition accuracies exceeding 99% for single- and two-hand gestures. Building on this, Zhang et al.[173] demonstrated that such systems could detect minute vibrations of the chest and mouth during speech. These non-contact gesture and voice control methods of human-computer interactions open new avenues for remote control and alternatives to traditional microphones. Furthermore, Li et al.[174] addressed a significant challenge in continuous health monitoring by designing a modular metasurface that can dynamically filter out noise from body movements (Fig. 7(d)). This enables more accurate and reliable tracking of vital signs, such as respiration patterns.

Collectively, these state-of-the-art applications highlight the transition of metasurface technology from a static tool for signal manipulation to a dynamic, perception-aware platform for sophisticated human sensing. Despite the promise of actively tunable wave manipulation at the subwavelength scale, most experimental demonstrations remain at GHz frequencies, owing to the practical ease of addressing individual meta-atoms. While nanofabrication capabilities are continuously evolving, considering the visible light operation of a 1 cm^2 metasurface, a reasonably sized 400 nm pitch would necessitate over 600 million addressable meta-atoms in such a small footprint. Increasing the pitch could relieve these requirements, however, at the cost of additional undesired diffraction modes. Although various novel strategies of post-fabrication modulation of optical metasurfaces have been proposed, the precise control of the optical properties of individual nanoscale meta-atoms is still a formidable hardware engineering challenge.

5 Perspectives & conclusions

5.1 Emerging frontiers & grand challenges

5.1.1 Energy efficient AI

While this review has focused on the development of AI for use in metaphotonic design and systems, the enormous power consumption of current electronics-based AI is a problem that could be also solved with optics and photonics for sustainable, low-power, on-device computation[175,176]. The training of a large AI model has the potential to cost millions of kilowatt-hours of electricity, and reports of users using the words 'please' and 'thank you' costing companies millions of dollars in compute during inference highlight the critical concerns of sustainable AI. Metaphotonics offers a pathway to enable orders-of-magnitude reductions in energy consumption by shifting key stages of the AI pipelines such as feature extraction, convolution, and encoding into the optical domain. Since metasurfaces are also fabricated using the same CMOS processes at electronic chips, extensive research has already been undertaken for on-chip integration[177], and analog computing[178–181]. Recent work has shown that optical front-end encoders, implemented by multi-channel meta-imagers, can perform convolution and feature-extraction operations in parallel while working at the speed of light, substantially off-loading the computational burden from electronic processors[182–184]. This has been shown to reduce the required calculations by 5 orders of magnitude[183] while maintaining high accuracy. In the microwave region, self-powered metasurfaces powered by stray waves have been confirmed[185]. Such opto-electronic metaphotonic devices could play a transformative role in enabling energy-efficient, on-device AI computation, with profound effects for the next generation of portable, intelligent systems.

5.1.2 Neuromorphic computing

As actively programmable metasurfaces have been demonstrated at GHz wavelengths, their miniaturization to optical wavelengths, fueled by advancements in nanofabrication[186], could open the doorway for neuromorphic metaphotonics[187,188]. Rather than being limited by the traditional von Neumann architecture, inspired by the structure and dynamics of the human brain, neuromorphic computing is particularly well-suited for low-power applications such as real-time decision-making, edge intelligence, and in-sensor processing[189]. In parallel, diffractive neural networks based on metasurfaces have been explored for optical information processing[190–192], enabling linear, parallel computations. Although these networks suffer from a lack of optical nonlinearities, one of the key components in learning complex distributions in DNNs, the flexibility of programmable metasurfaces to control light at will provides a strong foundation for further research. Temporal programmability without the need for nonlinear materials

has been verified[193], while spiking neural networks with reconfigurable metasurfaces have enabled event-driven control suitable for low-latency tasks[194].

5.1.3 Quantum metaphotonics

Photons provide an exciting proposition in the quest for scalable quantum systems due to their long coherence times at room temperature and on-chip scalability for quantum computing and communication in particular. As a powerful alternative to traditional superconducting qubits, photonic systems can access high-dimensional qubits, known as qudits, by harnessing the various quantum properties of photons such as polarization, direction, orbital angular momentum, and frequency[195]. While metasurfaces have been applied for the creation, manipulation, and detection of single and entangled photons from various sources, AI could offer an additional advancement in the design and development of quantum metasurfaces. Furthermore, the potential for quantum-inspired AI algorithms or quantum machine learning using metasurfaces is still yet to be extensively explored[196].

5.1.4 Data constraints & standardization

The Internet has provided an unprecedented dataset for human-curated knowledge in the form of text and images, which has been expertly leveraged to create powerful LLMs that are being implemented into natural language agents[197]. However, in the field of metaphotonics, the curation of such large datasets has been generally left to the individual lab or research team with no standards set for data sharing. Therefore, there is a distinct lack of large, diverse, and high-quality datasets for training, such as the classic MNIST or ImageNet dataset. Here, we would like to highlight an attempt to address this issue from the Fan group at Stanford[198], who have introduced a repository of simulated datasets with the goal of hosting a nanophotonic version of ImageNet. This problem is multifaceted however, since groups around the world have access to different materials and fabrication facilities, while often focusing on specific applications that require expert know-how for physical realization, beyond what is included in a simulated dataset. With standardized datasets, and inspiration from the AI community, benchmarking becomes possible through reference design tasks, i.e., standardized optimization challenges that allow researchers to objectively compare different AI architectures with the same dataset. It has been shown that multidimensional benchmarks are the most effective at pushing the state-of-the-art and also facilitate industry-academia collaboration to actively shape the research landscape[199].

5.1.5 Generalization & transferability

Beyond the availability of data, a critical limitation in current AI-assisted metaphotonics is the lack of model transferability. The majority of inverse design networks are single use, trained on specific parameters, such as the meta-atom material, height, and wavelength range. If the constraints change because a new material becomes available or a new fabrication technique allows for a larger aspect ratio structure, for example, the model typically suffers a catastrophic drop in accuracy and must be retrained from scratch. This rigidity contrasts sharply with modern AI trends, where models pre-trained on vast datasets can be adapted to new tasks with minimal fine-tuning, distillation, or transfer learning. To address this, future research must move toward the development of metaphotonic foundation models. Rather than memorizing the response of specific geometric libraries, such models could be trained on massive, multi-material physics simulations to learn the underlying operator of Maxwell's equations. Achieving this would enable few-shot or zero-shot learning, where a pre-trained model could predict the behavior of a completely new material platform or wavelength regime[200,201] using only a handful of reference simulations, drastically reducing the computational cost of deploying AI in new experimental settings.

5.1.6 Trainability of active systems

While programmable metasurfaces offer the potential for real-time adaptation, training AI models to control them presents unique challenges not found in static designs. Current approaches often train models on idealized analytical curves of active elements (e.g., liquid crystals), which fail to capture experimental realities such as hysteresis, thermal drift, and non-uniform voltage responses. This leads to a simulation-to-reality gap where the AI model fails when deployed on the physically realized metasurface. To overcome this, in-situ training is required, where the AI learns directly from the hardware output. However, this creates a data bottleneck for training, since unlike digital simulations which can be parallelized over multiple computers, physical experiments are serial and limited by the modulation speed of the device and the readout speed of the detector. As a solution, digital twins that can update a simulation model in real-time to match the physical device, could enable rapid, accurate offline training for programmable systems.

5.1.7 Addressing the simulation-to-reality gap

Although the promise of end-to-end optimized metasurface systems has been proven to somewhat overcome design limitations, the mismatch between high performance designs in simulation and experiment still poses additional challenges. Various AI implementations of inverse lithography have been proposed to improve the shortcomings of nanofabrication[202]. Fully connected AI models with multiple expert agents that take care of the design, optimization, fabrication, and even the experimental characterization of metaphotonic systems could provide an exciting new pathway for AI to autonomously enhance the real-world performance of optical devices, following the footprints of current

developments in AI chip design in industry[203].

The general 'black box' nature of AI models is a huge limitation in machine learning and AI in scientific research. However, optics has historically been an enabler for advancements in science and technology. Therefore, understanding the inner workings of a well-trained metaphotonic model through XAI could not only improve the interpretability and reliability of such models but could also hold the key to uncovering new nanoscale physics through metaphotonics or design principles that extend beyond human intuition.

5.2 Conclusions

In this review, we have highlighted the key advancements and impact of AI on metaphotonics, from the basics of data-driven simulations to fully automated systems that sense and adapt to their surroundings in real time. Early demonstrations of AI for the inverse design of metasurfaces[45,204] proved its potential using linear DNNs, generative models such as GANs and autoencoders. However, the development from science to technology requires real-world challenges to be addressed[22]. Limitations in data collection, model generalization, and interpretability provide research directions that could be influential in the future. Scalable nanofabrication is a bottleneck in the commercialization of metasurfaces, while nanoimprint lithography in roll-to-plate and roll-to-roll systems have been demonstrated[8,186], large scale fabrication and meta-atom level modulation remain key engineering hurdles that could require the collaboration between industry and academia, across various fields. AI could play a leading role in the optimization and control of the design and fabrication processes for real-world applications, potentially overcoming these hurdles. The integration of AI to analyze and interpret how metasurfaces interact with light for the creation of next generation sensing and imaging applications open new possibilities in metaphotonics at the system level and could alleviate the need for highly trained experts to perform measurements. This has been exemplified recently by end-to-end optimized systems, and autonomous metasurfaces that are able to actively reconfigure their properties based on external stimuli, all controlled by AI. With the potential of XAI to uncover new physics at the nanoscale, LLMs for interactive design systems, and on-chip photonics for optical and quantum computing, the active research area of AI-enhanced metasurfaces provides a powerful intersection between two state-of-the-art technologies for fundamental research and technology development.

References

1. Ha ST, Li QT, Yang JKW et al. Optoelectronic metadevices. *Science* **386**, eadm7442 (2024).
2. Cui TJ, Zhang S, Alù A et al. Roadmap on electromagnetic metamaterials and metasurfaces. *J Phys Photonics* **6**, 032502 (2024).
3. Yu NF, Genevet P, Kats MA et al. Light propagation with phase discontinuities: generalized laws of reflection and refraction. *Science* **334**, 333–337 (2011).
4. Kim Y, Lee J, Kim WS et al. Millisecond-level electrically switchable metalens for adaptive rotational depth mapping and diffraction-limited imaging. *Opto-Electron Adv* **9**, 250216 (2026).
5. Pan CF, Wang H, Wang HS et al. 3D-printed multilayer structures for high–numerical aperture achromatic metalenses. *Sci Adv* **9**, eadj9262 (2023).
6. Badloe T, Kim Y, Kim J et al. Bright-field and edge-enhanced imaging using an electrically tunable dual-mode metalens. *ACS Nano* **17**, 14678–14685 (2023).
7. Li C, Jang J, Badloe T et al. Arbitrarily structured quantum emission with a multifunctional metalens. *eLight* **3**, 19 (2023).
8. Choi M, Kim J, Moon S et al. Roll-to-plate printable RGB achromatic metalens for wide-field-of-view holographic near-eye displays. *Nat Mater* **24**, 535–543 (2025).
9. Xing ZY, Lin ZL, Liu N et al. Monolithic spin-multiplexing metalens for dual-functional imaging. *Laser Photonics Rev* **19**, 2401993 (2025).
10. So S, Kim J, Badloe T et al. Multicolor and 3D holography generated by inverse-designed single-cell metasurfaces. *Adv Mater* **35**, 2208520 (2023).
11. Kim J, Im JH, So S et al. Dynamic hyperspectral holography enabled by inverse-designed metasurfaces with oblique helicoidal cholesterics. *Adv Mater* **36**, 2311785 (2024).
12. Liu ZY, Gao H, Ma TG et al. Broadband spin and angle co-multiplexed waveguide-based metasurface for six-channel crosstalk-free holographic projection. *eLight* **4**, 7 (2024).
13. Yang WH, Xiao SM, Song QH et al. All-dielectric metasurface for high-performance structural color. *Nat Commun* **11**, 1864 (2020).
14. Wang HC, Martin OJF. Polarization-controlled chromo-encryption. *Adv Opt Mater* **11**, 2202165 (2023).
15. Zhang W, Wang HT, Wang H et al. Nanoscale 3D printing of glass photonic crystals with near-unity reflectance in the visible spectrum. *Sci Adv* **11**, eadv0267 (2025).
16. Zhang W, Min JK, Wang H et al. Printing of 3D photonic crystals in Titania with complete bandgap across the visible spectrum. *Nat Nanotechnol* **19**, 1813–1820 (2024).
17. Badloe T, Kim J, Kim I et al. Liquid crystal-powered Mie resonators for electrically tunable photorealistic color gradients and dark blacks. *Light Sci Appl* **11**, 118 (2022).
18. Silver D, Hubert T, Schrittwieser J et al. A general reinforcement learning algorithm that masters chess, shogi, and Go through self-play. *Science* **362**, 1140–1144 (2018).
19. Lambert N. Reinforcement learning from human feedback. arXiv: 2504.12501 (2025). https://doi.org/10.48550/arXiv.2504.12501.
20. Voulodimos A, Doulamis N, Doulamis A et al. Deep learning for computer vision: a brief review. *Comput Intell Neurosci* **2018**, 7068349 (2018).
21. Stanford University. *2025 AI Index Report. Stanford Institute for Human-Centered AI (HAI)*. (2025).
22. Brongersma ML, Pala RA, Altug H et al. The second optical metasurface revolution: moving from science to technology. *Nat Rev Electr Eng* **2**, 125–143 (2025).
23. Zhelyeznyakov MV, Brunton S, Majumdar A. Deep learning to accelerate scatterer-to-field mapping for inverse design of dielectric metasurfaces. *ACS Photonics* **8**, 481–488 (2021).
24. So S, Rho J. Designing nanophotonic structures using conditional deep convolutional generative adversarial networks. *Nanophotonics* **8**, 1255–1261 (2019).
25. Trisno J, Wang H, Wang HT et al. Applying machine learning to the optics of dielectric nanoblobs. *Adv Photonics Res* **1**, 2000068 (2020).
26. Zhang N, Gao F, Wang RD et al. Deep-learning empowered customized chiral metasurface for calibration-free biosensing. *Adv Mater* **37**, 2411490 (2025).
27. Tran TV, Nanthakumar SS, Zhuang XY. Deep learning-based framework for the on-demand inverse design of metamaterials with

arbitrary target band gap. *npj Artif Intell* **1**, 2 (2025).
28. Jing GQ, Wang PP, Wu HS et al. Neural network-based surrogate model for inverse design of metasurfaces. *Photonics Res* **10**, 1462–1471 (2022).
29. Wiecha PR, Muskens OL. Deep learning meets nanophotonics: a generalized accurate predictor for near fields and far fields of arbitrary 3D nanostructures. *Nano Lett* **20**, 329–338 (2020).
30. Augenstein Y, Repän T, Rockstuhl C. Neural operator-based surrogate solver for free-form electromagnetic inverse design. *ACS Photonics* **10**, 1547–1557 (2023).
31. Kang C, Seo J, Jang I et al. Adjoint method-based Fourier neural operator surrogate solver for wavefront shaping in tunable metasurfaces. *iScience* **28**, 111545 (2025).
32. Scarselli F, Gori M, Tsoi AC et al. The graph neural network model. *IEEE Trans Neural Netw* **20**, 61–80 (2009).
33. Khoram E, Wu ZC, Qu YR et al. Graph neural networks for metasurface modeling. *ACS Photonics* **10**, 892–899 (2023).
34. Kuhn L, Repän T, Rockstuhl C. Exploiting graph neural networks to perform finite-difference time-domain based optical simulations. *APL Photonics* **8**, 036109 (2023).
35. Pestourie R, Mroueh Y, Nguyen TV et al. Active learning of deep surrogates for PDEs: application to metasurface design. *npj Comput Mater* **6**, 164 (2020).
36. Weiss K, Khoshgoftaar TM, Wang DD. A survey of transfer learning. *J Big Data* **3**, 9 (2016).
37. Qu YR, Jing L, Shen YC et al. Migrating knowledge between physical scenarios based on artificial neural networks. *ACS Photonics* **6**, 1168–1174 (2019).
38. Jiang L, Li XZ, Wu QX et al. Neural network enabled metasurface design for phase manipulation. *Opt Express* **29**, 2521–2528 (2021).
39. Han X, Fan ZY, Liu ZY et al. Inverse design of metasurface optical filters using deep neural network with high degrees of freedom. *InfoMat* **3**, 432–442 (2021).
40. Xi JW, Shen J, Chow MT et al. Deep-learning assisted polarization holograms. *Adv Opt Mater* **12**, 2202663 (2024).
41. Barati Sedeh H, George RC, Lai FX et al. Toward the meta-atom library: experimental validation of machine learning-based Mietronics. *Adv Photonics* **7**, 036004 (2025).
42. Lee C, Rho J. Benchmarking optimization methods enabling efficient designs for diverse nanophotonic applications. *Adv Opt Mater* **13**, 2500195 (2025).
43. Zhang YX, Pu MB, Jin JJ et al. Crosstalk-free achromatic full Stokes imaging polarimetry metasurface enabled by polarization-dependent phase optimization. *Opto-Electron Adv* **5**, 220058 (2022).
44. Marzban R, Abiri H, Pestourie R et al. HiLAB: a hybrid inverse-design framework. arXiv: 2505.17491 (2025). https://doi.org/10.48550/arXiv.2505.17491
45. Keawmuang H, Hu SQ, Badloe T et al. Hybrid frameworks integrating deep learning and optimization methods for inverse design in nanophotonics. *ACS Appl Mater Interfaces* **17**, 33259–33270 (2025).
46. Chen YX, Zhang FY, Dang ZB et al. Chiral detection of biomolecules based on reinforcement learning. *Opto-Electron Sci* **2**, 220019 (2023).
47. Hemayat S, Moayed Baharlou S, Sergienko A et al. Integrating deep convolutional surrogate solvers and particle swarm optimization for efficient inverse design of plasmonic patch nanoantennas. *Nanophotonics* **13**, 3963–3983 (2024).
48. Li Y, Zhang Y, Wang Y et al. Multifunctional metasurface inverse design based on ultra-wideband spectrum prediction neural network. *Adv Opt Mater* **12**, 2302657 (2024).
49. Ma W, Cheng F, Xu YH et al. Probabilistic representation and inverse design of metamaterials based on a deep generative model with semi-supervised learning strategy. *Adv Mater* **31**, 1901111 (2019).
50. Liu ZC, Zhu DY, Rodrigues SP et al. Generative model for the inverse design of metasurfaces. *Nano Lett* **18**, 6570–6576 (2018).
51. Stanley KO. Compositional pattern producing networks: a novel abstraction of development. *Genet Program Evolvable Mach* **8**, 131–162 (2007).
52. Arjovsky M, Chintala S, Bottou L. Wasserstein GAN. arXiv: 1701.07875 (2017). https://doi.org/10.48550/arXiv.1701.07875.
53. Zhang ZZ, Yang CC, Qin YF et al. Diffusion probabilistic model based accurate and high-degree-of-freedom metasurface inverse design. *Nanophotonics* **12**, 3871–3881 (2023).
54. Dai MN, Jiang Y, Yang F et al. A surrogate-assisted extended generative adversarial network for parameter optimization in free-form metasurface design. *Neural Netw* **180**, 106654 (2024).
55. Yang HL, Yang CC, Li HB. Enhancing high-degree-of-freedom meta-atom design precision and speed with a tandem generative network. *ACS Photonics* **12**, 1184–1195 (2025).
56. Park C, Kim S, Jung AW et al. Sample-efficient inverse design of freeform nanophotonic devices with physics-informed reinforcement learning. *Nanophotonics* **13**, 1483–1492 (2024).
57. Blanchard-Dionne AP, Martin OJF. Teaching optics to a machine learning network. *Opt Lett* **45**, 2922–2925 (2020).
58. Jiang JQ, Fan JA. Global optimization of dielectric metasurfaces using a physics-driven neural network. *Nano Lett* **19**, 5366–5372 (2019).
59. Ha YL, Luo Y, Pu MB et al. Physics-data-driven intelligent optimization for large-aperture metalenses. *Opto-Electron Adv* **6**, 230133 (2023).
60. Lyu JB, Zhu T, Zhou Y et al. Inverse design for material anisotropy and its application for a compact X-cut TFLN on-chip wavelength demultiplexer. *Opto-Electron Sci* **2**, 230038 (2023).
61. Lim J, Psaltis D. MaxwellNet: physics-driven deep neural network training based on Maxwell's equations. *APL Photonics* **7**, 011301 (2022).
62. Medvedev V, Erdmann A, Rosskopf A. Physics-informed deep learning for 3D modeling of light diffraction from optical metasurfaces. *Opt Express* **33**, 1371–1384 (2025).
63. Li ZY, Pestourie R, Lin Z et al. Empowering metasurfaces with inverse design: principles and applications. *ACS Photonics* **9**, 2178–2192 (2022).
64. Shao GC, Zhou TK, Yan T et al. Reliable, efficient, and scalable photonic inverse design empowered by physics-inspired deep learning. *Nanophotonics* **14**, 2799–2810 (2025).
65. Gao Y, Chen W, Li FJ et al. Meta-attention deep learning for smart development of metasurface sensors. *Adv Sci* **11**, 2405750 (2024).
66. Ma W, Liu ZC, Kudyshev ZA et al. Deep learning for the design of photonic structures. *Nat Photonics* **15**, 77–90 (2021).
67. Zhang TN, Kee CY, Ang YS et al. Deep learning-based design of broadband GHz complex and random metasurfaces. *APL Photonics* **6**, 106101 (2021).
68. Kudyshev ZA, Kildishev AV, Shalaev VM et al. Machine-learning-assisted metasurface design for high-efficiency thermal emitter optimization. *Appl Phys Rev* **7**, 021407 (2020).
69. Yan JH, Yi JL, Ma CR et al. MetasurfaceViT: a generic AI model for metasurface inverse design. arXiv: 2504.14895 (2025). https://doi.org/10.48550/arXiv.2504.14895.
70. Zhang ZZ, Yang CC, Qin YF et al. Addressing high-performance data sparsity in metasurface inverse design using multi-objective optimization and diffusion probabilistic models. *Opt Express* **32**, 40869–40885 (2024).
71. Ding KY, Zhou Q, Chen MY et al. Deep learning empowered parallelized metasurface computed tomography snapshot spectral imaging. *Adv Mater* **37**, 2419383 (2025).
72. Grbčić L, Park M, Elzouka M et al. Inverse design of photonic surfaces via multi fidelity ensemble framework and femtosecond laser processing. *npj Comput Mater* **11**, 35 (2025).
73. Tanriover I, Lee D, Chen W et al. Deep generative modeling and inverse design of manufacturable free-form dielectric metasurfaces. *ACS Photonics* **10**, 875–883 (2023).
74. Terekhov P, Chang SY, Rahman T et al. Enhancing metasurface fabricability through minimum feature size enforcement. *Nanophotonics* **13**, 3147–3154 (2024).
75. Sang D, Xu MF, Pu MB et al. Toward high-efficiency ultrahigh numerical aperture freeform metalens: from vector diffraction

theory to topology optimization. *Laser Photonics Rev* **16**, 2200265 (2022).
76. Zhou Y, Shao YX, Mao CK et al. Inverse-designed metasurfaces with facile fabrication parameters. *J Opt* **26**, 055101 (2024).
77. Ueno A, Lin HI, Yang F et al. Dual-band optical collimator based on deep-learning designed, fabrication-friendly metasurfaces. *Nanophotonics* **12**, 3491–3499 (2023).
78. Pestourie R, Pérez-Arancibia C, Lin Z et al. Inverse design of large-area metasurfaces. *Opt Express* **26**, 33732–33747 (2018).
79. Li ZY, Pestourie R, Park JS et al. Inverse design enables large-scale high-performance meta-optics reshaping virtual reality. *Nat Commun* **13**, 2409 (2022).
80. Jia YT, Qian C, Fan ZX et al. A knowledge-inherited learning for intelligent metasurface design and assembly. *Light Sci Appl* **12**, 82 (2023).
81. Zhou Y, Mao CK, Gershnabel E et al. Large-area, high-numerical-aperture, freeform metasurfaces. *Laser Photonics Rev* **18**, 2300988 (2024).
82. Zhu EZ, Zong Z, Li EJ et al. Frequency transfer and inverse design for metasurface under multi-physics coupling by Euler latent dynamic and data-analytical regularizations. *Nat Commun* **16**, 2251 (2025).
83. Xu Y, Li F, Gu JQ et al. Spectral transfer-learning-based metasurface design assisted by complex-valued deep neural network. *Adv Photonics Nexus* **3**, 026002 (2024).
84. Yang GT, Xiao QX, Zhang ZL et al. Exploring AI in metasurface structures with forward and inverse design. *iScience* **28**, 111995 (2025).
85. Chen W, Sun R, Lee D et al. Generative inverse design of metamaterials with functional responses by interpretable learning. *Adv Intell Syst* **7**, 2400611 (2025).
86. You GF, Qian C, Tan SR et al. Driving deep-learning-based metasurface design with Kramers-Kronig relations. *Phys Rev Appl* **22**, L041002 (2024).
87. Breiman L. Random forests. *Mach Learn* **45**, 5–32 (2001).
88. Kim M, Park H, Shin J. Nanophotonic device design based on large language models: multilayer and metasurface examples. *Nanophotonics* **14**, 1273–1282 (2025).
89. Ma TG, Wang HZ, Guo LJ. OptoGPT: a foundation model for inverse design in optical multilayer thin film structures. *Opto-Electron Adv* **7**, 240062 (2024).
90. Chen MK, Liu XY, Sun YN et al. Artificial intelligence in meta-optics. *Chem Rev* **122**, 15356–15413 (2022).
91. Hu XM, Xu WZ, Fan QB et al. Metasurface-based computational imaging: a review. *Adv Photonics* **6**, 014002 (2024).
92. Qin J, Jiang SB, Wang ZS et al. Metasurface micro/nano-optical sensors: principles and applications. *ACS Nano* **16**, 11598–11618 (2022).
93. Wiecha PR, Lecestre A, Mallet N et al. Pushing the limits of optical information storage using deep learning. *Nat Nanotechnol* **14**, 237–244 (2019).
94. Tittl A, John-Herpin A, Leitis A et al. Metasurface-based molecular biosensing aided by artificial intelligence. *Angew Chem Int Ed* **58**, 14810–14822 (2019).
95. Lin SJ, Chen J, Liu WT et al. Detection of biomarkers using terahertz metasurface sensors and machine learning. *Appl Opt* **62**, 1027–1034 (2023).
96. Meng JJ, Balendhran S, Sabri Y et al. Smart mid-infrared metasurface microspectrometer gas sensing system. *Microsyst Nanoeng* **10**, 74 (2024).
97. Russell BJ, Meng JJ, Crozier KB. Mid-infrared gas classification using a bound state in the continuum metasurface and machine learning. *IEEE Sens J* **23**, 22389–22398 (2023).
98. Li HL, Kim JT, Kim JS et al. Metasurface-incorporated optofluidic refractive index sensing for identification of liquid chemicals through vision intelligence. *ACS Photonics* **10**, 780–789 (2023).
99. Wekalao J, Mandela N, Apochi O et al. Nanoengineered graphene metasurface surface Plasmon resonance sensor for precise hemoglobin detection with AI-assisted performance prediction. *Plasmonics* **20**, 3161–3184 (2024).
100. Badloe T, Yang Y, Lee S et al. Artificial intelligence-enhanced metasurfaces for instantaneous measurements of dispersive refractive index. *Adv Sci* **11**, 2403143 (2024).
101. Lei YS, Guo YH, Pu MB et al. Multispectral scattering imaging based on metasurface diffuser and deep learning. *Phys Status Solidi (RRL) – Rapid Res Lett* **16**, 2100469 (2022).
102. John-Herpin A, Kavungal D, von Mücke L et al. Infrared metasurface augmented by deep learning for monitoring dynamics between all major classes of biomolecules. *Adv Mater* **33**, 2006054 (2021).
103. Yang J, Wen BH, Ye XY et al. Deep learning-assisted molecular classification and concentration prediction by imaging of a large-area metasurface with spatially gradient geometry. *Adv Intell Syst* **6**, 2300353 (2024).
104. Lin CH, Huang SH, Lin TH et al. Metasurface-empowered snapshot hyperspectral imaging with convex/deep (CODE) small-data learning theory. *Nat Commun* **14**, 6979 (2023).
105. Barkey M, Büchner R, Wester A et al. Pixelated high-Q metasurfaces for in situ biospectroscopy and artificial intelligence-enabled classification of lipid membrane photoswitching dynamics. *ACS Nano* **18**, 11644–11654 (2024).
106. Yesilkoy F, Arvelo ER, Jahani Y et al. Ultrasensitive hyperspectral imaging and biodetection enabled by dielectric metasurfaces. *Nat Photonics* **13**, 390–396 (2019).
107. Faraji-Dana M, Arbabi E, Kwon H et al. Hyperspectral imager with folded metasurface optics. *ACS Photonics* **6**, 2161–2167 (2019).
108. Zhang LD, Zhou C, Liu BF et al. Real-time machine learning–enhanced hyperspectro-polarimetric imaging via an encoding metasurface. *Sci Adv* **10**, eadp5192 (2024).
109. Makarenko M, Burguete-Lopez A, Wang QZ et al. Real-time hyperspectral imaging in hardware via trained metasurface encoders. In *2022 IEEE/CVF Conference on Computer Vision and Pattern Recognition (CVPR)* 12682–12692 (IEEE, 2022). http://doi.org/10.1109/CVPR52688.2022.01236.
110. Kim JH, Hong IP. An optimization approach based on separated latent space for inverse design of metasurfaces. *IEEE Antennas Wirel Propag Lett* **23**, 2135–2139 (2024).
111. Singh S, Kumar R, Panda SS et al. Deep-learning enabled photonic nanostructure discovery in arbitrarily large shape sets *via* linked latent space representation learning. *Digital Discovery* **3**, 1612–1623 (2024).
112. Ren ZH, Zhang ZX, Wei JX et al. Wavelength-multiplexed hook nanoantennas for machine learning enabled mid-infrared spectroscopy. *Nat Commun* **13**, 3859 (2022).
113. Yeung C, Tsai JM, King B et al. Elucidating the behavior of nanophotonic structures through explainable machine learning algorithms. *ACS Photonics* **7**, 2309–2318 (2020).
114. Li Y, Huang XJ, Liu SX et al. Metasurfaces for near-eye display applications. *Opto-Electron Sci* **2**, 230025 (2023).
115. Fröch JE, Colburn S, Brady DJ et al. Computational imaging with meta-optics. *Optica* **12**, 774 (2025).
116. Wang FL, Zhao SQ, Wen YZ et al. High efficiency visible achromatic metalens design via deep learning. *Adv Opt Mater* **11**, 2300394 (2023).
117. Dong YX, Zheng BW, Li H et al. Achromatic single metalens imaging via deep neural network. *ACS Photonics* **11**, 1645–1656 (2024).
118. Chu CH, Hsu CC, Luo Y et al. Enhancing metalens imaging quality using CGAN-based deep learning approach. *J Opt Microsyst* **5**, 024504 (2025).
119. Chen QK, Zhou JC, Pian SJ et al. Hybrid meta-optics enabled compact augmented reality display with computational image reinforcement. *ACS Photonics* **11**, 3794–3803 (2024).
120. Dong YX, Zheng BW, Yang F et al. Full-color, wide field-of-view metalens imaging via deep learning. *Adv Opt Mater* **13**, 2402207 (2025).
121. Liu Y, Li WD, Xin KY et al. Ultra-wide FOV meta-camera with transformer-neural-network color imaging methodology. *Adv Photonics* **6**, 056001 (2024).
122. Kim J, Seong J, Kim W et al. Scalable manufacturing of high-index atomic layer–polymer hybrid metasurfaces for metaphotonics in the visible. *Nat Mater* **22**, 474–481 (2023).
123. Seo J, Jo J, Kim J et al. Deep-learning-driven end-to-end metalens

imaging. *Adv Photonics* **6**, 066002 (2024).
124. Zhang PS, Yan LH, Liang HW et al. RGB achromatic metalens for neural network-enhanced high resolution digital imaging. *Laser Photonics Rev* **19**, e00460 (2025).
125. Liu XY, Li WY, Yamaguchi T et al. Stereo vision meta-lens-assisted driving vision. *ACS Photonics* **11**, 2546–2555 (2024).
126. Chen MK, Liu XY, Wu YF et al. A meta-device for intelligent depth perception. *Adv Mater* **35**, 2107465 (2023).
127. Liu XY, Zhang JC, Leng BR et al. Edge enhanced depth perception with binocular meta-lens. *Opto-Electron Sci* **3**, 230033 (2024).
128. Tan SY, Yang F, Boominathan V et al. 3D imaging using extreme dispersion in optical metasurfaces. *ACS Photonics* **8**, 1421–1429 (2021).
129. Yang B, Ma DN, Liu WW et al. Deep-learning-based colorimetric polarization-angle detection with metasurfaces. *Optica* **9**, 217–220 (2022).
130. Liu XY, Chen MK, Chu CH et al. Underwater binocular meta-lens. *ACS Photonics* **10**, 2382–2389 (2023).
131. Jiang H, Chen YZ, Guo WY et al. Metasurface-enabled broadband multidimensional photodetectors. *Nat Commun* **15**, 8347 (2024).
132. Peng YF, Choi S, Padmanaban N et al. Neural holography with camera-in-the-loop training. *ACM Trans Graph* (*TOG*) **39**, 185 (2020).
133. Kim J, Seong J, Yang Y et al. Tunable metasurfaces towards versatile metalenses and metaholograms: a review. *Adv Photonics* **4**, 024001 (2022).
134. Peng YY, Zhang JW, Zhou XT et al. Metalens in improving imaging quality: advancements, challenges, and prospects for future display. *Laser Photonics Rev* **18**, 2300731 (2024).
135. Jeon D, Shin K, Moon SW et al. Recent advancements of metalenses for functional imaging. *Nano Converg* **10**, 24 (2023).
136. Tseng E, Colburn S, Whitehead J et al. Neural nano-optics for high-quality thin lens imaging. *Nat Commun* **12**, 6493 (2021).
137. Pinilla S, Fröch JE, Miri Rostami SR et al. Miniature color camera via flat hybrid meta-optics. *Sci Adv* **9**, eadg7297 (2023).
138. Park Y, Kim Y, Kim C et al. End-to-end optimization of metalens for broadband and wide-angle imaging. *Adv Opt Mater* **13**, 2402853 (2025).
139. Fröch JE, Chakravarthula P, Sun JP et al. Beating spectral bandwidth limits for large aperture broadband nano-optics. *Nat Commun* **16**, 3025 (2025).
140. Fisher S, Arya G, Majumdar A et al. End-to-end metasurface design for temperature imaging via broadband Planck-radiation regression. *Adv Opt Mater* **13**, 2402498 (2025).
141. Wei W, Tang P, Shao JZ et al. End-to-end design of metasurface-based complex-amplitude holograms by physics-driven deep neural networks. *Nanophotonics* **11**, 2921–2929 (2022).
142. Noh J, Kim J, Rho J. Overcoming information sparsity in metasurfaces for full-color holography via end-to-end design. *Nano Lett* **25**, 11398–11405 (2025).
143. Yin YY, Jiang Q, Wang HB et al. Multi-dimensional multiplexed metasurface holography by inverse design. *Adv Mater* **36**, 2312303 (2024).
144. Liu XJ, Ma ZY, Zhang DS et al. Hypermultiplexed off-chip hologram by on-chip integrated metasurface. *Adv Opt Mater* **12**, 2401169 (2024).
145. Gopakumar M, Lee GY, Choi S et al. Full-colour 3D holographic augmented-reality displays with metasurface waveguides. *Nature* **629**, 791–797 (2024).
146. Choi S, Jang C, Lanman D et al. Synthetic aperture waveguide holography for compact mixed-reality displays with large étendue. *Nat Photonics* **19**, 854–863 (2025).
147. Jang C, Bang K, Chae M et al. Waveguide holography for 3D augmented reality glasses. *Nat Commun* **15**, 66 (2024).
148. Lin Z, Pestourie R, Roques-Carmes C et al. End-to-end metasurface inverse design for single-shot multi-channel imaging. *Opt Express* **30**, 28358–28370 (2022).
149. Zhang QB, Yu ZQ, Liu XY et al. End-to-end joint optimization of metasurface and image processing for compact snapshot hyperspectral imaging. *Opt Commun* **530**, 129154 (2023).
150. Lin Z, Roques-Carmes C, Pestourie R et al. End-to-end nanophotonic inverse design for imaging and polarimetry. *Nanophotonics* **10**, 1177–1187 (2021).
151. Xu SY, Chi CR, Zheng S et al. End-to-end optimization of single-shot monocular metasurface camera for RGBD imaging. *Opt Commun* **566**, 130691 (2024).
152. Kim G, Kim Y, Yun J et al. Metasurface-driven full-space structured light for three-dimensional imaging. *Nat Commun* **13**, 5920 (2022).
153. Choi E, Kim G, Yun J et al. 360° structured light with learned metasurfaces. *Nat Photonics* **18**, 848–855 (2024).
154. Badloe T, Lee J, Seong J et al. Tunable metasurfaces: the path to fully active nanophotonics. *Adv Photonics Res* **2**, 2000205 (2021).
155. Qian C, Kaminer I, Chen HS. A guidance to intelligent metamaterials and metamaterials intelligence. *Nat Commun* **16**, 1154 (2025).
156. Schurig D, Mock JJ, Justice BJ et al. Metamaterial electromagnetic cloak at microwave frequencies. *Science* **314**, 977–980 (2006).
157. Qian C, Zheng B, Shen YC et al. Deep-learning-enabled self-adaptive microwave cloak without human intervention. *Nat Photonics* **14**, 383–390 (2020).
158. Zhen Z, Qian C, Jia YT et al. Realizing transmitted metasurface cloak by a tandem neural network. *Photonics Res* **9**, B229–B235 (2021).
159. Wang ZD, Qian C, Lin PJ et al. 3D intelligent cloaked vehicle equipped with thousand-level reconfigurable full-polarization metasurfaces. *Adv Mater* **36**, 2400797 (2024).
160. Wang HL, Zhang YK, Cheng YT et al. A self-adaptive switchable transparency/invisibility cloak based on programmable metasurface. *Laser Photonics Rev* **19**, 2500057 (2025).
161. Fan ZX, Qian C, Jia YT et al. Homeostatic neuro-metasurfaces for dynamic wireless channel management. *Sci Adv* **8**, eabn7905 (2022).
162. Jiang RZ, Ma Q, Gu Z et al. Simultaneously intelligent sensing and beamforming based on an adaptive information metasurface. *Adv Sci* **11**, 2306181 (2024).
163. Liu W, Wang SR, Dai JY et al. Arbitrarily rotating polarization direction and manipulating phases in linear and nonlinear ways using programmable metasurface. *Light Sci Appl* **13**, 172 (2024).
164. Ma H, Kim JS, Choe JH et al. Deep-learning-assisted reconfigurable metasurface antenna for real-time holographic beam steering. *Nanophotonics* **12**, 2415–2423 (2023).
165. Zhang L, Chen XQ, Liu S et al. Space-time-coding digital metasurfaces. *Nat Commun* **9**, 4334 (2018).
166. Wang SR, Chen ZY, Chen SN et al. Simplified radar architecture based on information metasurface. *Nat Commun* **16**, 6505 (2025).
167. Chen XQ, Zhang L, Zheng YN et al. Integrated sensing and communication based on space-time-coding metasurfaces. *Nat Commun* **16**, 1836 (2025).
168. Zhao Y, Li L, Lanteri S et al. Dynamic metasurface control using Deep Reinforcement Learning. *Math Comput Simul* **197**, 377–395 (2022).
169. Hu JZ, Zhang HL, Bian KG et al. MetaSensing: intelligent metasurface assisted RF 3D sensing by deep reinforcement learning. *IEEE J Sel Areas Commun* **39**, 2182–2197 (2021).
170. Hu SG, Li MY, Xu JW et al. Electromagnetic metamaterial agent. *Light Sci Appl* **14**, 12 (2025).
171. Luo XG. Digital optics and optical intelligent agent. *Appl Phys Lett* **127**, 010501 (2025).
172. Ma Q, Gu Z, Gao XX et al. Intelligent hand-gesture recognition based on programmable topological metasurfaces. *Adv Funct Mater* **35**, 2411667 (2025).
173. Zhang HR, Ruan HX, Zhao HT et al. Microwave speech recognizer empowered by a programmable metasurface. *Adv Sci* **11**, 2309826 (2024).
174. Li XY, Chen L, Qin SL et al. BioMeta: modular reprogrammable metasurface for noninvasive human respiration monitoring. *Nanophotonics* **14**, 981–991 (2025).
175. Bente I, Taheriniya S, Lenzini F et al. The potential of multidimensional photonic computing. *Nat Rev Phys* **7**, 439–450 (2025).
176. Kalinin KP, Gladrow J, Chu JQ et al. Analog optical computer for AI inference and combinatorial optimization. *Nature* **645**, 354–361

(2025).
177. Zheng CL, Ni PN, Xie YY et al. On-chip light control of semiconductor optoelectronic devices using integrated metasurfaces. *Opto-Electron Adv* **8**, 240159 (2025).
178. Badloe T, Lee S, Rho J. Computation at the speed of light: metamaterials for all-optical calculations and neural networks. *Adv Photonics* **4**, 064002 (2022).
179. Abou-Hamdan L, Marinov E, Wiecha P et al. Programmable metasurfaces for future photonic artificial intelligence. *Nat Rev Phys* **7**, 331–347 (2025).
180. Tang P, Jeon Y, Li XT et al. Switchable bright-field imaging and corner detection with an electrically tunable metalens. *Adv Opt Mater* **13**, 2500981 (2025).
181. Kim Y, Tang P, Jung C et al. Topological vortex transition induced by spin hall effect of light for tunable humidity sensing and imaging. *Laser Photonics Rev* **19**, e00581 (2025).
182. Huang LC, Tanguy QAA, Fröch JE et al. Photonic advantage of optical encoders. *Nanophotonics* **13**, 1191–1196 (2024).
183. Choi M, Xiang JL, Wirth-Singh A et al. Transferable polychromatic optical encoder for neural networks. *Nat Commun* **16**, 5623 (2025).
184. Zheng HY, Liu Q, Kravchenko II et al. Multichannel meta-imagers for accelerating machine vision. *Nat Nanotechnol* **19**, 471–478 (2024).
185. Zhou YJ, Wu XB, Cai XD et al. Smart meta-device powered by stray microwave energies: a green approach to shielding external interference and detection. *Appl Energy* **378**, 124770 (2025).
186. Yang Y, Jeon Y, Dong ZG et al. Nanofabrication for nanophotonics. *ACS Nano* **19**, 12491–12605 (2025).
187. Brunner D, Shastri BJ, Al Qadasi MA et al. Roadmap on neuromorphic photonics. arXiv: 2501.07917 (2025). https://doi.org/10.48550/arXiv.2501.07917.
188. Li RJ, Gong YH, Huang H et al. Photonics for neuromorphic computing: fundamentals, devices, and opportunities. *Adv Mater* **37**, 2312825 (2025).
189. Roy K, Jaiswal A, Panda P. Towards spike-based machine intelligence with neuromorphic computing. *Nature* **575**, 607–617 (2019).
190. He C, Zhao D, Fan F et al. Pluggable multitask diffractive neural networks based on cascaded metasurfaces. *Opto-Electron Adv* **7**, 230005 (2024).
191. Liu XY, Chen MK, Tsai DP. Photonic meta-neurons. *Laser Photonics Rev* **18**, 2300456 (2024).
192. Liu C, Ma Q, Luo ZJ et al. A programmable diffractive deep neural network based on a digital-coding metasurface array. *Nat Electron* **5**, 113–122 (2022).
193. You GF, Qian C, Chen HS. Parallel nonlinear neuromorphic computing with temporal encoding. arXiv: 2506.17261 (2025). https://doi.org/10.48550/arXiv.2506.17261
194. Tsinos CG, Boulogeorgos AAA, Tsiftsis TA. NeuroRIS: neuromorphic-inspired metasurfaces. *IEEE Wirel Commun Lett* **13**, 1878–1882 (2024).
195. Liu GX, Zhou WJ, Gromyko D et al. Single-photon generation and manipulation in quantum nanophotonics. *Appl Phys Rev* **12**, 011308 (2025).
196. Li QY, Liang MG, Liu SQ et al. Phase reconstruction via metasurface-integrated quantum analog operation. *Opto-Electron Adv* **8**, 240239 (2025).
197. Touvron H, Martin L, Stone K et al. Llama 2: open foundation and fine-tuned chat models. arXiv: 2307.09288 (2023). https://doi.org/10.48550/arXiv.2307.09288
198. Metanet. http://metanet.stanford.edu/.
199. Martínez-Plumed F, Barredo P, hÉigeartaigh SÓ et al. Research community dynamics behind popular AI benchmarks. *Nat Mach Intell* **3**, 581–589 (2021).
200. Zhang C, Chen L, Lin ZL et al. Tantalum pentoxide: a new material platform for high-performance dielectric metasurface optics in the ultraviolet and visible region. *Light Sci Appl* **13**, 23 (2024).
201. Zhou HX, Xing ZY, Hu YH et al. Compact generation of ultraviolet structured light via low-loss dielectric metasurfaces. *Adv Opt Mater* e01940 (2025). doi: 10.1002/adom.202501940.
202. Yang YX, Liu KX, Gao YH et al. Advancements and challenges in inverse lithography technology: a review of artificial intelligence-based approaches. *Light Sci Appl* **14**, 250 (2025).
203. Liu MJ, Ene TD, Kirby R et al. ChipNeMo: domain-adapted LLMs for chip design. arXiv: 2311.00176 (2023). https://doi.org/10.48550/arXiv.2311.00176
204. So S, Badloe T, Noh J et al. Deep learning enabled inverse design in nanophotonics. *Nanophotonics* **9**, 1041–1057 (2020).

Acknowledgements

This work was supported by the Alchemist Project grant funded by Korea Planning & Evaluation Institute of Industrial Technology (KEIT) & the Korea Government (MOTIE) (Project Number: 1415185027, 20019169), and the Regional Innovation System & Education (RISE) program through the Sejong RISE Center, funded by the Ministry of Education (MOE) and the Sejong City, Republic of Korea (2025-RISE-08-001). S.S. acknowledges the NRF Sejong Science fellowship (NRF-2022R1C1C2009430) funded by the Ministry of Science and ICT (MSIT) of the Korean Government. H. Wang acknowledges the support from National Natural Science Foundation of China (NSFC, Grant No. 606HWRC2025117001), the Fundamental Research Funds for the Central Universities (Grant No. 501RCQD2025117002), and the Research Funding of Hangzhou International Innovation Institute, Beihang University (Grant No. 015733207-000001). J.K.W.Y. acknowledges funding support from the National Research Foundation of Singapore (NRFS), under its Competitive Research Programme award NRF-CRP30-2023-0003.

Author contributions

All authors confirmed the final manuscript.

Competing interests

The authors declare no competing financial interests.